Simulation of the Structure and Properties of the Polyethylene Crystal Surface

by

John L. Wilhelmi

B.S., Stanford University (1991)

Submitted to the Department of Chemical Engineering
in partial fulfillment of the requirements for the degree of

Master of Science in Chemical Engineering

at the

MASSACHUSETTS INSTITUTE OF TECHNOLOGY

February 1996

Author .....
Department of Chemical Engineering
February 7, 1996

Certified by .....
Gregory C. Rutledge
J.R. Mares Associate Professor
Thesis Supervisor

Accepted by .....
Professor Robert E. Cohen
Chairman, Committee for Graduate Students

Simulation of the Structure and Properties of the Polyethylene Crystal Surface

by

John L. Wilhelmi

Submitted to the Department of Chemical Engineering
on February 7, 1996, in partial fulfillment of the
requirements for the degree of
Master of Science in Chemical Engineering

Abstract

The structures and thermodynamic properties of the lateral surface of extended-chain polyethylene crystals were simulated using consistent quasi-harmonic lattice dynamics and Monte Carlo methods.

Using quasi-harmonic lattice dynamics, the structures and properties of the (100), (010), and (110) lateral surfaces of extended-chain polyethylene crystals between 0 K and 300 K were determined by vibrational free energy minimizations. Slight rotations of the outermost chains from their corresponding orientations in the bulk were observed at the crystal-vacuum interface. These deviations from bulk structure were confined to the first three molecular layers (approximately 10 Å) at the surface. Surface free energy calculations found the (110) surface to be the most stable over the entire temperature range modeled, with free energies ranging from 95.4 erg/cm^2 to 103.5 erg/cm^2, at temperatures of 0 K and 300 K, respectively. Surface free energies of the (100) and (010) surfaces were found to be at least 15% higher than the (110) surface, with the (100) surface slightly more stable than the (010) surface, over all temperatures considered. Surface free energy increases as the density of chains at the surface decreases. Intermolecular potential energy accounted for over 80% of the surface free energy at low temperatures; at higher temperatures, excess entropy accounted for almost half of the surface free energy. The surface free energy was determined predominantly by deviations in lattice mode frequencies from those of the bulk. The accuracy of these results is limited by the validity of the harmonic approximation, which is expected to be reasonably valid to temperatures between 1/3 and 2/3 of the melting temperature for modeling the surfaces of polymer crystals.

Investigative Monte Carlo simulations of the thermal motions of rigid chains in a crystalline slab were conducted to determine structural data to supplement the lattice dynamics results. Monte Carlo simulations in the NVT ensemble generated results similar to those found in previous studies, but could only be run by restricting the motions of chains to a volume centered at a fixed lattice point, an assumption which is shown here to severely limit the phase space accessible to the system. Such assumptions were not necessary for NPT simulations, and realistic results were ob-

served at pressures between 5 and 10 atomspheres. For all Monte Carlo simulations, significant rotational and translational disorder was observed in the outermost crystalline layer, with the magnitude of disorder decreasing with depth into the crystal. Disorder also diminished with decreased temperature. Lattice expansion of roughly 2–3% was observed in the outermost crystal layer.

The computed results, most notably the surface free energies and the comparative mobility of surface chains, are expected to be valuable in future predictions on the behavior of polymer crystallization kinetics.

Thesis Supervisor: Gregory C. Rutledge
Title: J.R. Mares Associate Professor

Acknowledgments

I would like to thank my thesis committee, especially my advisor, Prof. Gregory C. Rutledge, for their technical contributions to my thesis work. The daily advice given by Steve Foulger and Jeff Carbeck was also greatly appreciated.

In addition, there are many people, places, and things, that made my stay at MIT memorable, and all hold a special place in my heart: Cambridge Volleyball Association and the Boston Mets, Herring Cove beach, 1 Pilgrim Heights Road, "The Coven", and, above all, Gary Furtado.

Contents

List of Figures

List of Tables

Chapter 1

Introduction

1.1 Background

It has been well established that linear, flexible chain polymers crystallized from dilute solution form lamellar crystals. Such crystals, as shown in Figure 1-1, have two distinct surfaces, known as lateral and fold surfaces. Since the prevalent kinetic

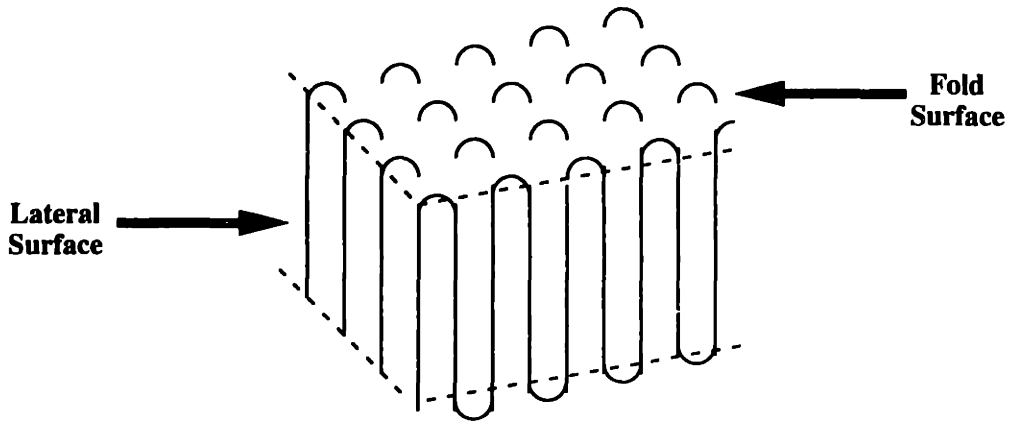

Figure 1-1: Surfaces observed in polymer crystals grown from dilute solution; only tight folds with adjacent reentry are shown.

theories of polymer crystallization postulate that crystal growth occurs through the addition of chain segments to the lateral surface, it is expected that the structure and properties of the lateral surface will have a strong influence on polymer crystal growth

behavior.[1-4] The properties of the lateral crystal surface are also of interest in understanding surface properties of crystals grown under pressure, epitaxially grown crystals, crystals of rigid polymers, or any other system in which the lateral surface may be macroscopically observed. However, to this date, few rigorous studies have been conducted to quantify the structure and properties of the lateral surface in crystalline polymers.[5-9]

1.2 Review of Previous Work

Of all the properties of the lateral crystal surface, the surface free energy has received the most attention, and many different values of the lateral surface free energy for polyethylene crystals have been reported in the literature. Most reported lateral surface free energies for polyethylene fall in the range 10-25 erg/cm^2[1, 4], and have been calculated from the following empirical equation proposed by Thomas and Staveley for computing surface free energies for atomic crystals [10]:

$$\sigma = \alpha \Delta H_f (a_o b_o)^{1/2} \tag{1.1}$$

where σ is the surface free energy, α is a proportionality constant found to range from 0.1–0.3 for atomic crystals, ΔH_f is the latent heat of fusion, and a_o and b_o are lattice spacing parameters. The empirical relation was derived by determining which surface free energy would best match theoretical predictions of crystallization kinetics to experimentally observed growth rates of atomic crystals.[10] Thus, the accuracy of the empirical relation is ultimately limited by the accuracy of the original experimental observations, and, more significantly, by the crystallization theory used in deriving surface free energies. Furthermore, the nature of polymer crystals (as shown in Figure 1-1) is inherently different from that of atomic crystals, and it is questionable whether the empirical relation can be selectively applied to the lateral surface for polymer crystals. Hoffman *et al.* have reported a lateral surface free energy for the polymer crystal-solvent interface of 14.6 erg/cm^2 based on both the Thomas and Staveley

approach (given in Equation 1.1) using n-octadecane as a surrogate for polyethylene, and on consistencies between observed crystal growth kinetics and the theoretical predictions of polymer crystal growth.[2] Recent studies on the crystallization kinetics of semi-rigid polymers have found that lateral surface free energies calculated using the Thomas and Staveley approach differ significantly from those predicted by polymer crystallization theory using experimentally observed crystal growth rates [8], but this inconsistency was attributed to the lack of applicability of secondary nucleation theory to semi-rigid polymer crystallization.

A commonly referenced surface free energy is 33.1 erg/cm^2 for the polyehtylene-vacuum interface, based on a contact angle study of low density polyethylene samples.[11, 12] However, it is expected that the exposed surface in the cited study contained significant amounts of amorphous polymer, and the surface free energy may differ considerably from that of the actual crystalline interface. Such problems in isolation of the lateral crystal surface from amorphous regions make experimental observations of lateral surface properties extremely difficult.

The use of computer simulation provides a means to probe the crystal surface without the associated difficulties encountered in experimental observations. Yamamoto *et al.* have investigated the nature of n-alkane crystal surfaces using Monte Carlo simulations of finite, lozenge-shaped lattices, and have observed significant disorder in the outermost two to three molecular layers of the crystal, with the magnitude of disorder becoming more pronounced with increased temperature.[5] The results of the study may be influenced by the shape of the crystal lattice examined, and by the neglect of thermal expansion over the temperature range 0–200 K. The study also confined the translational motion of molecules to a small region fixed at the crystalline lattice point; simulations considering molecular motions of arbitrary magnitude and direction were not stable.[5] Liang *et al.* have used molecular dynamics simulations to reach similar conclusions, but their study did not explicitly account for the hydrogens in the polyethlyene.[6] Karasawa, Dasgupta, and Goddard (KDG) have modeled the lateral surface properties of polyetheylene crystals using lattice dynamics simulations, and have computed 0 K surface free energies of 106.8 erg/cm^2 and 109.2 erg/cm^2,

for the (100) and (010) surfaces, respectively.[7] However, the KDG work did not report the structure of chains at the surface or the temperature dependence of the surface properties, and did not consider the effects of 0 K expansion. Furthermore, polyethylene crystals grown from dilute solution are known to exhibit primarily (110) growth fronts, but the properties of this surface were not treated.

1.3 Research Goals

The present study provides the first rigorous calculation of the temperature dependence of the structure and properties of the polyethylene lateral crystal surface, determined from first principles. This study uses a tiered modeling approach to find the free energy minimum structures of the (100), (010), and (110) lateral surfaces of extended-chain polyethylene crystals, up to temperatures of 300 K. Consistent quasi-harmonic lattice dynamics simulations are used to determine the low temperature behavior of the surfaces, and a Monte Carlo modeling approach has been developed to complement the findings of the lattice dynamics simulations, especially at higher temperatures. The simulation methodology used in this analysis is applicable to the study of the low temperature behavior of the lateral crystal surface of any polymer, provided an accurate force field exists for the polymer of interest.

The second section of this report presents the modeling approach and results of the consistent quasi-harmonic lattice dynamics study, and the third section details the model and results of the Monte Carlo simulations. The fourth section offers a discussion of the accuracy of the computed surface free energies and the relevance of these values to experimentally observable phenomena. The final section gives a summary of the present work and recommendations for future work in the analysis of the lateral crystal surface of polymers.

Chapter 2

Quasi-Harmonic Lattice Dynamics

The structure and properties of a thin crystalline slab of extended-chain polyethylene molecules were determined using consistent quasi-harmonic lattice dyanmics simulations. The lattice dynamics modeling approach is presented first, and is based largely on that used in a previous study of bulk crystalline polyethylene [13], adapted to simulate two dimensional structures. The vibrational free energy minimum structures and properties are then presented in the results section.

2.1 Modeling Approach

Consistent quasi-harmonic lattice dynamics was used to determine the structures which minimized the vibrational Gibbs free energy. The simulation cells used to generate the fine crystalline slab are described first, followed by a detailed summary of lattice dynamics theory, a discussion of the algorithm used to minimize the vibrational Gibbs free energy, and the equations used to calculate surface properties.

2.1.1 Generation of Crystalline Slab

The Cartesian coordinates of the atoms in the simulation cell were determined as follows. One atom in a reference chain at the center of the slab is fixed at the origin of the coordinate system, and $3N_{at} - 3$ coordinates are then required to place the

remaining atoms of the reference chain, where N_{at} is the number of atoms per chain in a unit cell ($N_{at} = 6$ for polyethylene). As an initial guess, the coordinates of the atoms in the reference chain are assigned the values previously computed for the bulk crystal.[13] The other chains in the simulation cell were assumed to be conformationally equivalent to the reference chain. The Cartesian coordinates of the atoms in all but the reference chain are determined by four additional chain packing parameters. Three translational offset parameters determine the placement of the chain center of mass within the simulation cell, and the chain setting angle determines the orientation of the plane of the chain backbone with respect to the *bc*-plane of the crystal. Since the force field used in this study (KDG force field, see next section) was parameterized to orthorhombic polyethylene crystals [7], the simulation cells in this study were confined to be orthorhombic, requiring three lattice parameters to characterize the simulation cell dimensions.

The simulation cell used to model the (100) surface is depicted in Figure 2-1. As shown, the surface simulation cell is much larger than the unit cell observed for bulk crystalline polyethylene. By considering periodic boundary conditions in the direction of the chain axis, extended chain crystals are modeled; and periodicity in the *b*-axis direction generates an infinite crystalline slab, with (100) surfaces exposed to vacuum on both sides. The (010) and (110) surfaces were similarly represented with appropriate changes in the simulation cell and the directions of the periodicity considered. Slab thicknesses of 50 Å were found to be sufficient to ensure non-interacting surfaces and attainment of bulk structures at the center of the simulation cell. As shown in Figure 2-2, simulations of thicker slabs did not change surface properties significantly. The number of molecular layers considered in the simulation cell for a given facet was determined by the quotient of the 50 Å minimum slab thickness and the spacing between molecular layers parallel to the crystal surface as determined from previous simulations of the bulk crystal.[13] A summary of this calculation for the different facets is shown in Table 2.1.

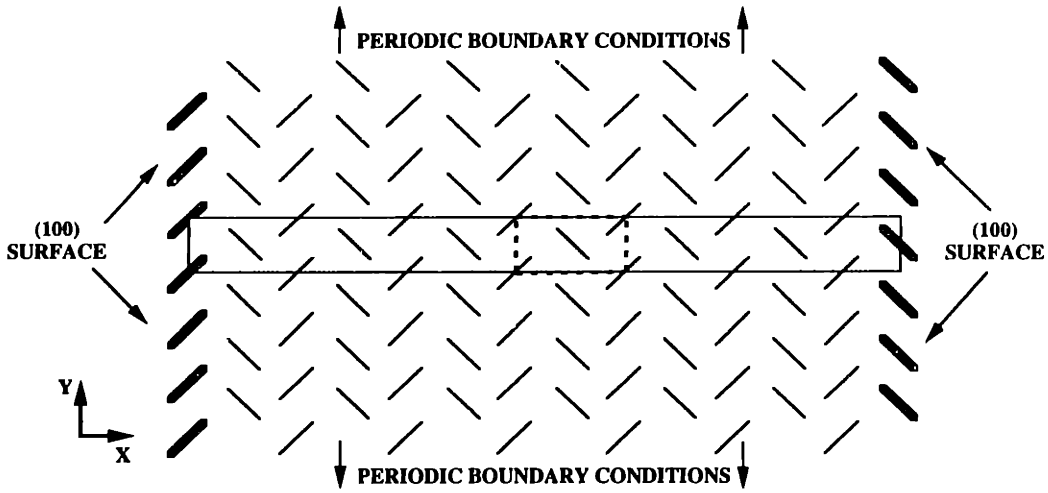

Figure 2-1: Representation of the thin molecular slab used to model (100) surfaces: diagonal lines are projections of chain backbones as viewed down the chain axis; bold lines denote chains which lie on the (100) surface; the dotted line indicates the bulk crystal unit cell; the shaded region marks the boundary of the simulation cell; and periodic boundary conditions are considered in the direction shown (and in the direction of the chain axis).

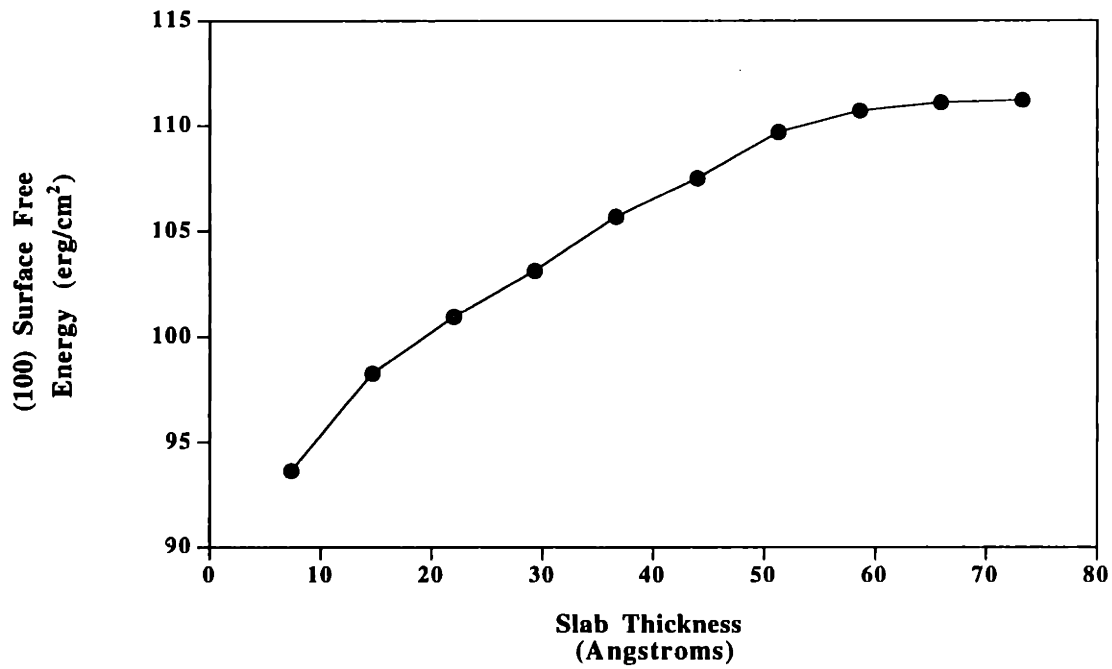

Figure 2-2: (100) Surface free energy, calculated at 0 K, as a function of slab thickness.

Crystal Facet	Interlayer Spacing (Å)	Layers in surface simulation cell
(100)	3.78	14
(010)	2.48	21
(110)	4.15	12

Table 2.1: Number of molecular layers considered in simulation cell for different surfaces modeled.

2.1.2 Lattice Dynamics Theory

Consistent quasi-harmonic lattice dynamics was used to determine the structures which minimize the vibrational Gibbs free energy, as calculated from:

$$G(T,P) = U(a) + A_{vib}(T,a) - PV(a) \tag{2.1}$$

where G is the vibrational Gibbs free energy, U is the minimum potential (electronic) energy for a slab of thickness a, A_{vib} is the vibrational Helmholtz free energy, P is the pressure, V is the volume of the simulation cell, and T is the simulation temperature. The remainder of this section discusses the computation of each term used in Equation 2.1, and the algorithm used to minimize the vibrational Gibbs free energy.

Electronic Energy

Electronic energies were evaluated using a Hessian-biased force field developed by KDG.[7] Electronic energies computed with the KDG force field consist of intermolecular and intramolecular contributions. The long range interactions, electrostatic and van der Waals, make up the intermolecular energies, and shorter range valence interactions are considered in the intramolecular energies. The KDG force field parameters were found to best fit quantum mechanical calculations for butane, experimental vibrational frequencies for butane, and experimental vibrational frequencies and structural parameters for polyethylene. The force field has been used to model phonon dispersion curves, specific heats, and thermal expansion parameters of bulk crystalline polyethylene to a high degree of accuracy.[7, 13] Even though the

force field was not specifically parameterized to surface properties, it should provide a good first approximation.

In previous bulk studies, long range interactions were evaluated using Ewald summations; however, analytical expressions for two dimensional Ewald summations are not available for interactions of the form $1/r^6$, the functional form of the dispersion energy in the KDG force field. Because of this, unit cell-based cutoffs were used to evaluate long range interactions in the surface simulations. Calculations on bulk crystalline polyethylene show that implementation of a 25 Å, unit cell-based cutoff is sufficient for evaluation of both electrostatic and dispersion energies to better than 0.01 kcal/mol accuracy (less than 0.02% and 0.002% error, respectively). KDG have suggested that long range interactions must be determined to better than 0.1 kcal/mol accuracy to "satisfactorily" predict bulk polyethylene unit cell structure.[14] Thus, 25 Å unit cell-based cutoffs were deemed sufficient for the present study. Simulations of the surface properties were carried out with cutoff distances as large as 35 Å, with no significant difference in results.

Vibrational Free Energy

Vibrational Helmholtz free energies were calculated using consistent quasi-harmonic lattice dynamics. The application of this computational approach to crystals and surfaces has been discussed thoroughly in the literature, and the salient features are presented here.[15-17] The success of this approach rests on the validity of the harmonic approximation, which assumes that normal mode motions of atoms in the crystal can be considered purely harmonic. Thus, the harmonic approximation constrains the potential energy surface to be parabolic in shape with respect to normal mode motions. Terms higher than second order in the expansion of the potential energy are neglected in the harmonic approximation. The quasi-harmonic approximation allows for the lattice parameters, and therefore the shape of the potential energy surface, to vary with temperature, leading to a first order prediction of the temperature dependence of structures and properties.

Previous studies on the application of the harmonic approximation to bulk crys-

tals suggest that this assumption is reasonably accurate up to 2/3 to 3/4 of the melting temperature.[18, 19] Unlike the atoms embedded in the bulk crystal, atoms near surfaces have fewer constraints on their motions, and anharmonic motions are expected to become prevalent at lower temperatures than for the corresponding bulk crystal. For example, lattice dynamics studies of the surfaces of noble gas crystals have suggested that anharmonic motions become prevalent at temperatures as low as one sixth the melting point.[20] In comparison to the noble gas crystals, the onset of anharmonicities in polymer crystals is expected to occur at higher temperatures due to the constraints on atomic motions imposed by the covalent bonds in the polymer chain. With these bounds in mind, reasonable validity of the harmonic approximation is anticipated in this study to a temperature intermediate between 1/3 and 2/3 of the melting temperature. As discussed later in this report, Monte Carlo methods do not rely on such approximations, and thus more accurately model the surface structure and properties at high temperatures.

Provided the atoms in the simulation cell are at their potential energy minimum positions, diagonalization of the dynamical matrix as a function of wave vector yields the frequencies of the 3N normal modes (where N is the number of atoms in the simulation cell). Terms in the dynamical matrix are dependent on the second derivatives of the potential energy with respect to atomic displacements, and these derivatives must be determined to a high degree of accuracy. Using this approach, the vibrational partition function for the system of quantized harmonic oscillators can be calculated as [21]:

$$\ln(Q_{qm}) = \sum_{\mathbf{k}}^{N_k} \sum_{i}^{3N} -\frac{\hbar\omega_i(\mathbf{k})}{2} - \ln\left(1 - \exp\left[-\frac{\hbar\omega_i(\mathbf{k})}{kT}\right]\right) \tag{2.2}$$

where Q_{qm} is the quantum mechanical vibrational partition function, the first summation is over all wave vectors $\mathbf{k}$, the second summation is over the normal modes i in the simulation cell, and $\omega_i(\mathbf{k})$ is the vibrational frequency of mode i for wave vector $\mathbf{k}$. Use of the quantum partition function allows for the correct representation of low temperature dynamics and zero-point energies. The previous work by KDG used the classical vibrational partition function, which does not account for such effects.[7]

In an infinite crystal, an infinite number of wave vectors characterize the motions of the atoms; however, the wave vectors spanning the first Brillioun zone are unique, and only a representative set of first Brillioun zone wave vectors is necessary for adequate evaluation of the vibrational partition function. The Brillioun zones for these surface studies are two dimensional. Vibrational frequencies were computed on a 4 × 6 mesh of wave vectors: 6 wave vectors along the reciprocal space axis corresponding to the chain axis in real space, and 4 wave vectors along the reciprocal space axis representing the axis lateral to the surface in real space. Calculations using a 6 × 8 intergration mesh generated very similar results.

Many thermodynamic properties can be calculated directly from the partition function using statistical mechanics.[21] For example, the vibrational Helmholtz free energy for a simulation cell can be calculated as:

$$A_{vib} = E_{vib} - TS_{vib} = -\frac{kT \ln Q_{qm}}{N_k} \tag{2.3}$$

where A_{vib} is the vibrational Helmholtz free energy, E_{vib} is the vibrational energy, S_{vib} is the vibrational entropy, T is the temperature, and N_k is the number of wave vectors considered in the calculation. Other thermodynamic properties, such as the heat capacity, can also be calculated from basic statistical mechanics relations.[21]

2.1.3 Free Energy Minimization Algorithm

The free energy minimization algorithm is shown schematically in Figure 2-3, and the strucure comprising the minimum in vibrational Gibbs free energy, as given by Equation 2.1, was determined as follows. For a given slab thickness a, the structure of minimum potential (electronic) energy was determined with respect to the following degrees of freedom: the $3N_{at} - 3$ Cartesian coordinates of the reference chain atoms, and the translational offset parameters and setting angles of the remaining chains. Assuming that the presence of the surface only perturbs the lattice spacing of chains in the direction normal to the surface, lattice periodicities in directions parallel to the surface were fixed at values characteristic of the bulk, as determined

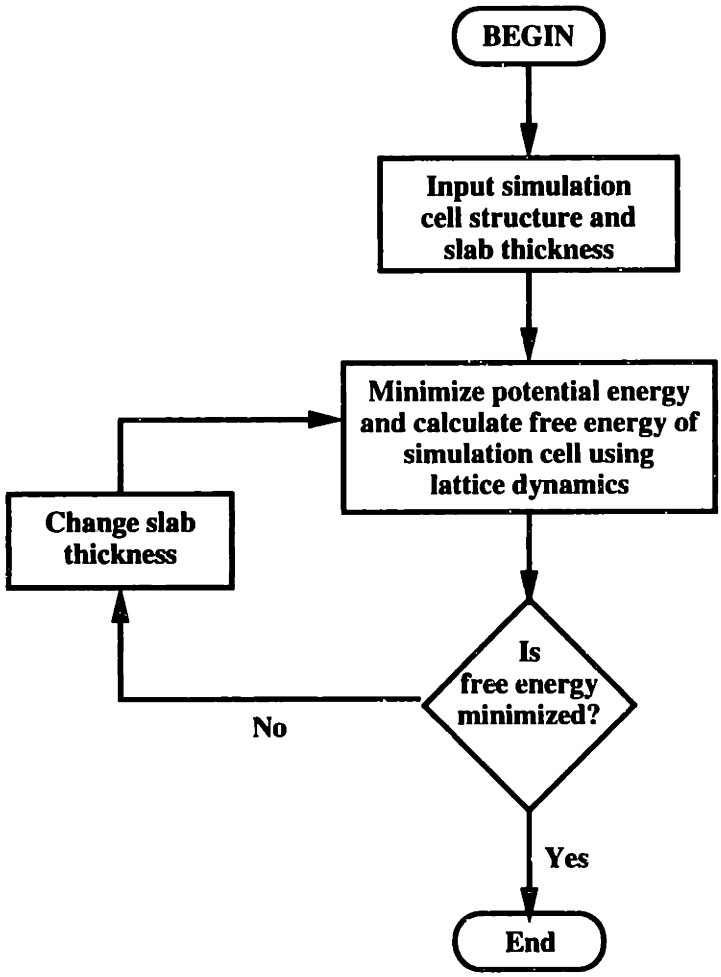

Figure 2-3: Flow chart depicting the free energy minimization algorithm used in consistent quasi-harmonic lattice dynamics modeling. The free energy minimum is determined after a thorough search over slab thicknesses.

from a quasi-harmonic analysis of the bulk crystal using the KDG force field.[13] In order to hold the slab thickness fixed, one degree of freedom specifying the translational distance between chains at opposite surfaces of the slab was held constant. Minimizations were performed using analytical derivatives and a quasi-Newton minimization algorithm.[22] At the calculated minimum in potential energy, the normal mode frequencies and corresponding vibrational free energy were determined from the vibrational partition function for a quantized collection of harmonic oscillators (see Equations 2.2 and 2.3). The slab thickness was then varied systematically, with repeated refinement of U and A_{vib}, to minimize G. At atmospheric pressure, the contribution of the pressure term (PV) is negligible in comparison to the sum of U and A_{vib}; thus, the pressure was set to zero in all cases. Using this approach, all results are calculated consistently from the force field alone, without the need of other experimental data as parameters in the calculations.

2.1.4 Computation of Surface Properties

The following equation was used to compute surface properties:

$$\mathcal{P} = \frac{P_{surf} - P_{bulk}}{A} \tag{2.4}$$

where $\mathcal{P}$ is the surface property, P_{surf} is the property of interest calculated for the surface simulation cell, P_{bulk} is the property calculated for a bulk unit cell having the same number of chains, and A is the surface area exposed. Surface free energies were calculated by replacing P_{surf} and P_{bulk} by the Gibbs free energy calculated for the respective systems. The previous equation was also used to determine the relative contributions of intermolecular potential energy, intramolecular potential energy, vibrational energy, and vibrational entropy to the calculated surface free energies.

2.2 Results

2.2.1 Vibrational Free Energy Minimum Structure

The free energy minimum structures of the surface simulation cells were found to have a large region in the center of the crystalline slab in which the structures of the chains were virtually identical to the structures obtained in analyses of the bulk crystal, and a much smaller region near the lateral surfaces in which the structure of the chains were observed to deviate slightly from the corresponding bulk structure. The observed structural deviations may have significant implications on previous studies which have assumed the structure of surface chains are not perturbed from their bulk values.[3, 9]

The structural feature most sensitive to the presence of a surface was a deviation in the setting angles in the chains in the outermost layers of the crystalline slab. In all cases, the outermost chains were found to rotate towards an orientation in which the plane of the chain backbone approaches an orientation closer to normal to the plane of the surface. Alternating counterrotations were observed in subsequent layers, limited to the 2–3 outermost layers, 0–10 Å, for all surfaces modeled. As an example, in Figure 2-4 the deviation in chain setting angles from their bulk values is plotted against the crystal layer (layer 1 being the surface), for the 0 K simulation of the (100), (010), and (110) surfaces. Structural deviations in the outermost layers were observed over the entire temperature range modeled. Studies of the surfaces of *n*-alkane crystals have also concluded that deviations in molecular structure are limited to the outermost two to three molecular layers [6, 5], and this interfacial depth has also been observed in simulations of the amorphous polymer-vacuum interface.[23] Although no constraints were placed on layer-to-layer spacing between chains in the direction normal to the surface, no significant departure from the spacing characteristic of the bulk was observed in any of the simulations, even for planes of chains close to the surface.

The structures determined from the consistent quasi-harmonic lattice dynamics calculations characterize only the vibrational free energy minimum structures, and

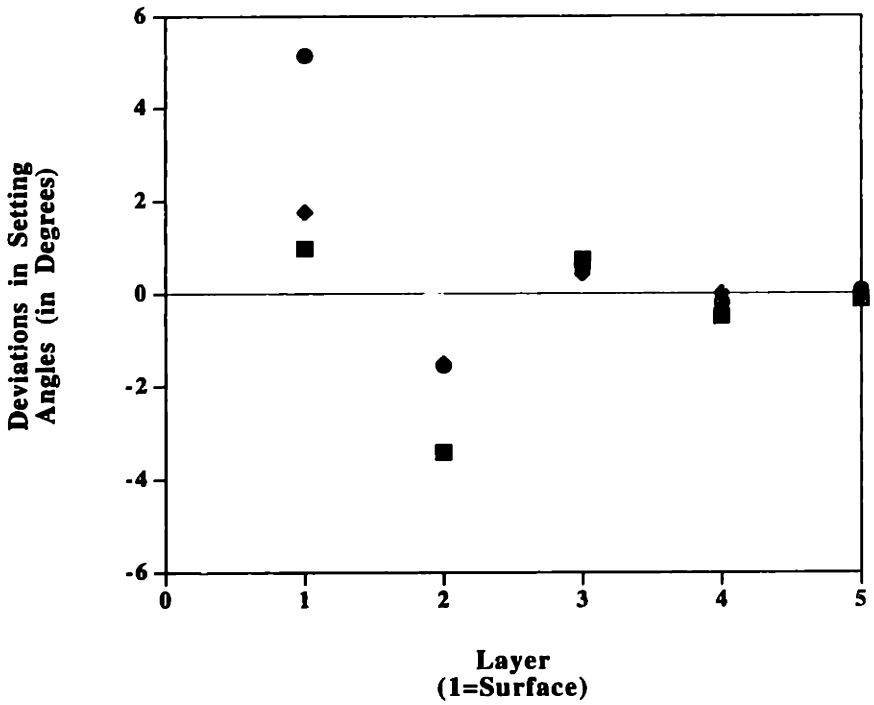

Figure 2-4: Results of chain structure for 0 K simulations. Deviations in chain setting angles from corresponding bulk values as a function of depth from the surface (layer 1 is the surface layer). Filled circles are for the (100) surface, filled diamonds for the (110) surface, and filled squares for the (010) surface.

chains, especially those at the surface, exhibit significant motions about these minimized structures. The nature of these motions was quantified using the Monte Carlo methods, and the results of the Monte Carlo simulations are presented in the next chapter.

2.2.2 Vibrational Frequency Spectrum

As properties of the surface simulation cell were calculated from the vibrational frequency spectrum using statistical mechanics, deviations in properties between the surface and bulk crystals should also be manifested in deviations in the vibrational frequency spectrum. In analyzing the frequency spectra, two classes of normal mode motions were considered: vibration of the lattice modes (frequencies below 300 cm^{-1} at the Brillioun zone center) and vibration of the higher frequency modes, to be collectively referred to as "intramolecular" modes in this paper.

To determine the impact of the surface on the vibrational frequency spectra, phonon dispersion curves were plotted for a surface simulation, and compared to the curves found for the simulation of a bulk polyethylene simulation cell of the same dimensions. For the (100) surface simulation cell shown in Figure 2-1, there are 252 normal modes—56 lattice and 196 intramolecular—characterizing the motions of the atoms. To illustrate the impact of the surface on lattice mode motions, phonon dispersion curves were plotted for one small class of lattice mode motions, transverse acoustical (TA, see ref. [7]) modes, and the results are shown in Figure 2-5, as calculated for the (100) surface simulation cell at 0 K.

As shown in plot (a) of Figure 2-5, the transverse acoustical modes for the bulk crystal converge to an energy of 268 cm^{-1} at the [0 0 $\frac{1}{2}$] point, in agreement with previous work by KDG.[7] The dispersion curves for the (100) surface simulation cell, displayed in plot (b) of Figure 2-5, are almost identical to the bulk, with the exception of two modes, labelled as surface modes, which have frequencies of 256 cm^{-1} at the [0 0 $\frac{1}{2}$] point. The surface modes converge to the bulk crystal modes at the center of the Brillioun zone, and deviate to lower frequencies with distance from the zone center, qualitatively consistent with previous simulated dispersion curves for

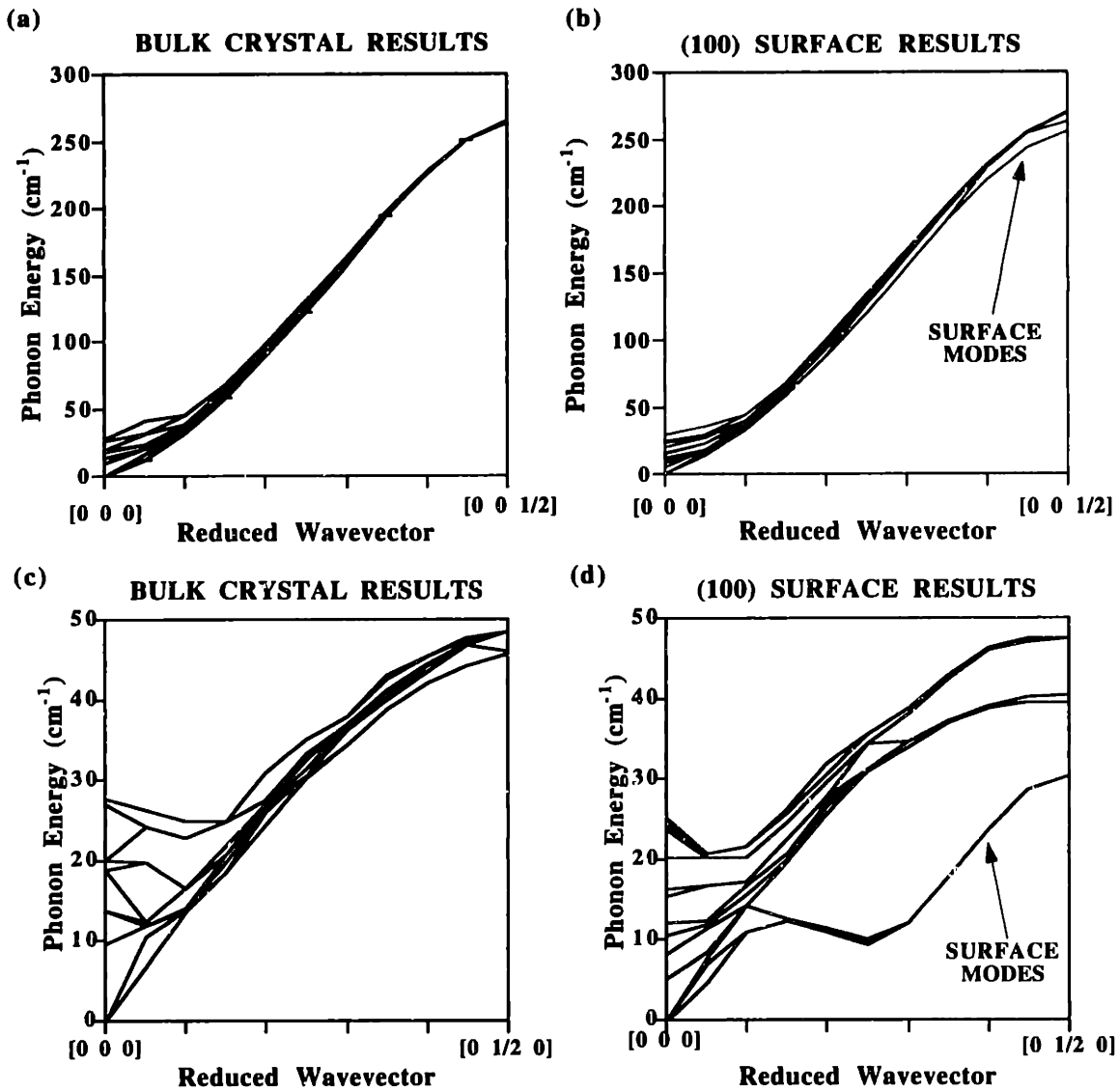

Figure 2-5: Phonon dispersion curves for the transverse acoustical modes of the (100) surface calculated at 0 K. The bulk and surface results along the [0 0 1], or chain axis, branch is shown in plots (a) and (b); and along the [0 1 0] branch in plots (c) and (d). Lower frequency, large amplitude surface modes are indicated.

a Lennard Jones crystalline slab.[24, 25] These lower frequency surface modes are characterized by large amplitude motion in the surface chains, with the amplitude of motion decaying with depth in the crystal, and a node of zero displacement at the center of the slab. This observation is consistent with early theoretical predictions of the Raman spectra in polyethylene.[26]

The [0 $\frac{1}{2}$ 0] branch of the transverse acoustical waves are shown in parts (c) and (d) of Figure 2-5 for the bulk and surface simulations, respectively. The waves for the bulk crystal converge at the [0 $\frac{1}{2}$ 0] point to either 48.7 cm^{-1} or 45.8 cm^{-1}. The behavior of this branch of the dispersion curves for bulk polyethylene crystals was not found in the literature. In the surface simulations, the branches of the dispersion curves were found to converge at the [0 $\frac{1}{2}$ 0] point to three frequencies: 47.7 cm^{-1}, 39.7 cm^{-1}, and 30.6 cm^{-1}. The highest frequency branch closely matches the behavior of the dispersion curve for the bulk crystal; the intermediate branch converges at a frequency slightly lower than that of the lower frequency bulk crystal branch; and the lowest frequency branch consists of two surface modes with significantly lower vibrational frequencies over all wave vectors considered. The depressed frequencies in the vibrational modes account for the surface thermodynamic properties calculated from the vibrational partition function.

Phonon dispersion curves were plotted for other groups of lattice mode motions, and for other surfaces and temperatures, and the same general effect was observed: the dispersion curves for the surface simulation cell closely matched that of the bulk, with the exception of usually two modes (semi-infinite slabs would have one surface mode[24]) with depressed frequencies. The deviation in these surface lattice modes account for a large fraction of the surface properties to be discussed in the next section. Similar comparisons were made for intramolecular modes, yet very small deviations were observed between the bulk and surface simulations. Thus, as will be shown in the next section, the contribution of intramolecular modes to the calculated properties was expected to be negligible.

2.2.3 Thermodynamic Properties

Surface properties were calculated using Equation 2.4. The 0 K surface free energies for the (100), (010), and (110) surfaces were found to be 109.7, 111.8, and 93.4 erg/cm^2, respectively. In comparison, the previous KDG work predicted surface free energies of 106.8 and 109.2 erg/cm^2 for the (100) and (010) surfaces, respectively.[7] The difference between these surface free energies is expected to be a result of zero-point energy effects, which were not addressed in the KDG work. KDG suggested that inclusion of such effects would most likely lead to a change of approximately 2% in their computed surface free energies[7], which is consistent with the values reported here.

The temperature dependence of the surface free energies is shown in Figure 2-6. As can be seen in the plot, the (110) surface is predicted to be the most stable

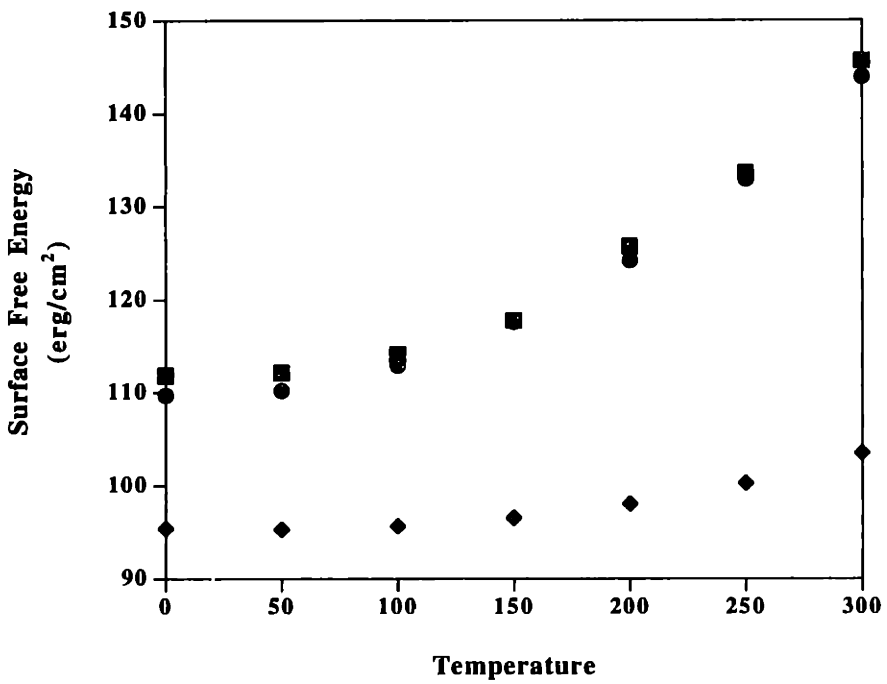

Figure 2-6: Surface free energy as a function of crystal growth face and temperature. Filled circles are for the (100) surface, filled diamonds for the (110) surface, and filled squares for the (010) surface.

over the entire temperature range considered. The (100) and (010) surfaces have significantly higher surface free energies, and the (100) surface is slightly more stable than the (010) surface over all temperatures modeled. The surface free energies predicted in this study are significantly higher than those found by Hoffman *et al.*; however, Hoffman's predictions of lateral surface free energies are characteristic of the crystal-solvent interface, and Hoffman notes that surface free energies for the crystal-vacuum interface are expected to be "considerably higher".[2] As shown in Figure 2-6, lateral surface energies are expected to increase with temperature, in agreement with the predictions of Hoffman *et al.*[2] It should be noted that the lateral surface free energy for all faces increases by at least 10% from 0 to 300 K, and, like the structural deviations noted earlier, this temperature dependence may have significant implications on previous studies which have assumed the lateral surface free energy to be independent of temperature.[27]

More detailed information on the thermodynamics of the surfaces can be obtained by considering the breakdown of the surface free energy into contributions from intramolecular potential energy, intermolecular potential energy, vibrational energy, and vibrational entropy. For all surfaces and temperatures, the intramolecular energy contribution to the surface free energy was found to be less than 2%. Since the intramolecular degrees of freedom in this study were determined by the reference chain located in the center of the slab, it was expected to find little deviations in intramolecular energies between the surface and bulk simulations. The temperature dependence of the other contributions to the surface free energy are displayed for all crystal facets in Figure 2-7. At lower temperatures, the intermolecular energy contribution dominates the surface free energy, and the entropic contribution is small, as expected. As the temperature increases, the entropy makes a significantly greater portion of the surface free energy. The contribution from vibrational energy remains roughly constant with temperature. In comparing the different faces, it is found that the added stability of the (110) surface is due to lower contributions from vibrational energy and entropy over the entire temperature range considered. This may be traced to the higher frequencies of the (110) surface modes (in comparison to the (100) and

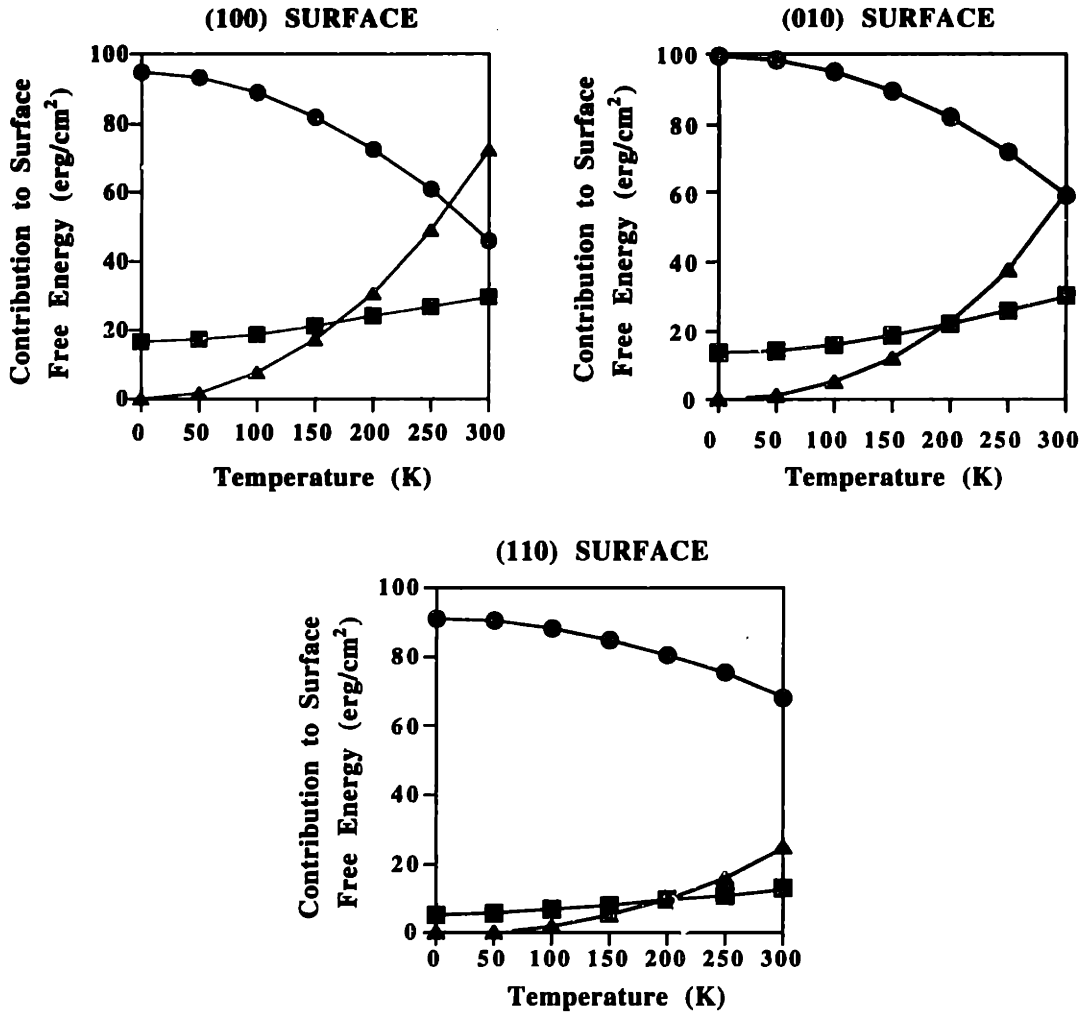

Figure 2-7: Breakdown of surface free energies for the (100), (010), and (110) lateral surfaces into contributions from intermolecular potential energy (filled circles), vibrational energy (filled squares), and vibrational "entropy" (filled triangles). The values shown for "entropy" are the absolute value of the product of the temperature and the vibrational entropy.

(010) surface modes) at the more densely packed surface.

The source of the excess vibrational free energy can be investigated further by considering the contributions from the lattice and intramolecular modes to the vibrational Helmholtz free energy. This was done by constructing the quantum partition function (see Equation 2.2) using only lattice mode frequencies, and using this modified partition function to evaluate properties. The results of such calculations are shown in Figure 2-8. Intermolecular potential energies are determined explicitly from

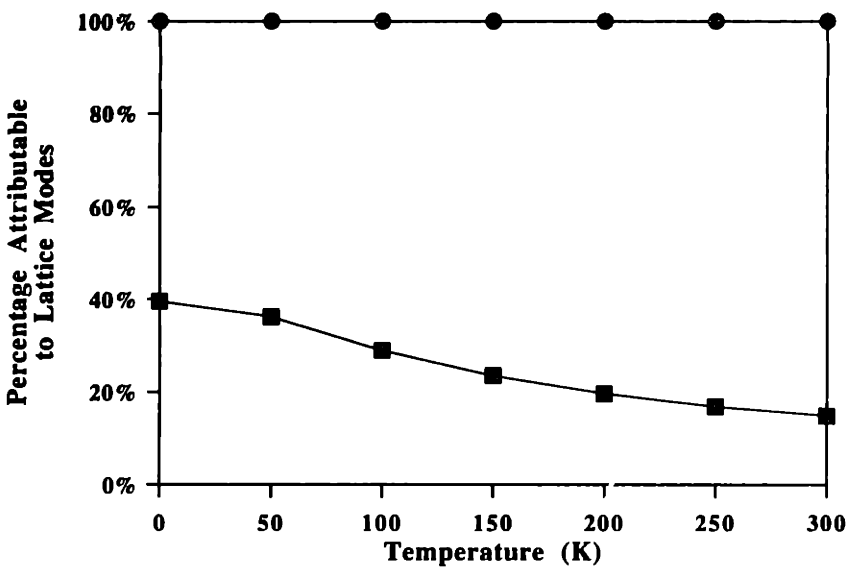

Figure 2-8: Contribution of lattice mode motions to the (100) surface vibrational energy (shown as filled squares) and (100) surface vibrational entropy (shown as filled circles) as a function of temperature.

the force field, and therefore cannot be separated into contributions from lattice and intramolecular modes. Over all temperatures considered, the lattice mode motions accounted for less than half of the surface vibrational energy, and virtually all of the surface vibrational entropy. This result, in conjunction with that shown in Figure 2-7, suggests that the temperature dependence of the calculated surface free energies is almost entirely due to the entropic effects associated with the excitation of lattice mode motions particular to the surface.

Chapter 3

Monte Carlo Simulations

Monte Carlo simulations can be used to estimate statistical mechanical ensemble averages through strategic sampling of the system phase space. In the present work, simulations are performed in the isothermal-isobaric, or NPT, ensemble using "Metropolis" sampling, a technique designed to ensure the most populated regions of phase space are thoroughly sampled.[28] The current approach was inspired by the study of Yamamoto *et al.* [5], which is reviewed first. This is followed by a detailed description of the present modeling approach, and discussion of preliminary results.

3.1 Review of Previous Attempt

The previous Monte Carlo study by Yamamoto *et al.* considered the thermal motions of n-alkane molecules in lozenge-shaped crystals, with lateral surfaces of the lozenge closely resembling the surface of extended-chain polyethylene crystals.[5] The simulations sampled phase space from the canonical, or NVT, ensemble, and considered the rotation and translation of rigid molecules about their lattice positions over the temperature range 100–200 K. The study examined the (100) and (110) surfaces of the finite crystal by using a simulation cell similar to that shown in Figure 3-1. The study found significant rotational and translational disorder for the molecules near the lateral crystal surface, with the magnitude of disorder becoming more pronounced at higher temperatures. In all cases, molecules at the (100) surface exhibited greater

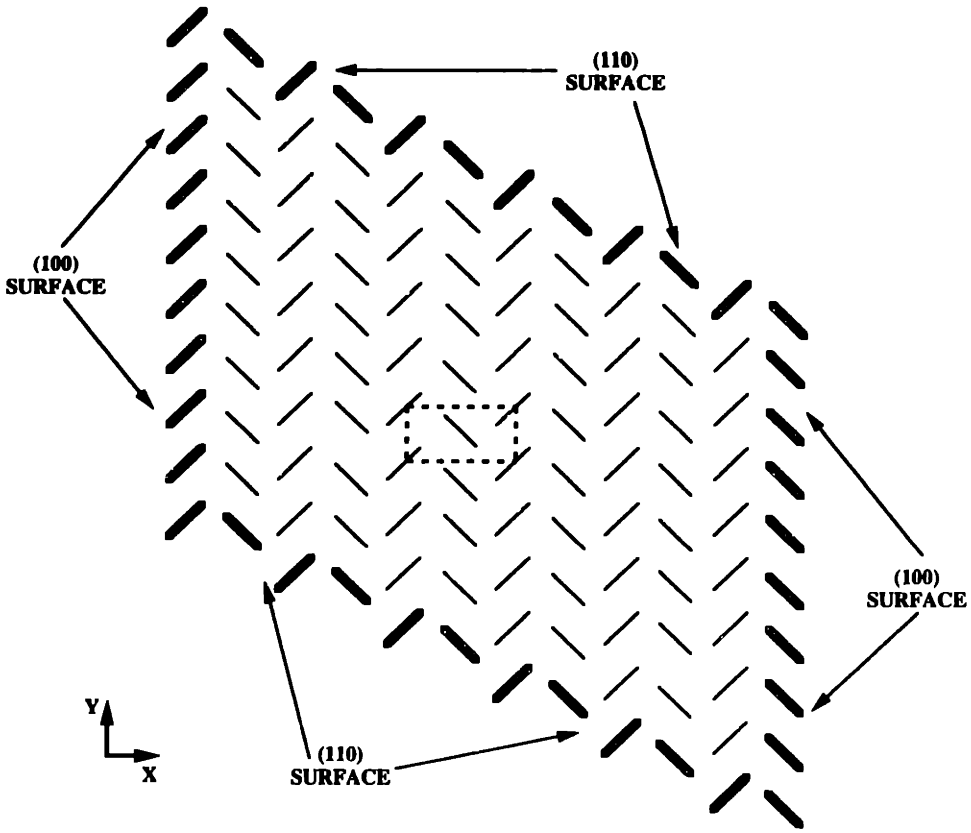

Figure 3-1: Simulation cell used by Yamamoto *et al.* for Monte Carlo analysis. Diagonal lines are projections of molecular backbones as viewed down the n-alkane axis; bold lines denote molecules which lie on the (100) or (110) surfaces; the dotted line indicates the bulk crystal unit cell; and no periodic boundary conditions are considered.

disorder than those at the (110) surface.

The results of the previous study rely on several key assumptions, some of which may come at the expense of the physics of the system. For example, translational motion of molecules was confined to 1 Å displacements about bulk crystal lattice sites, which may be viewed as effectively imposing a harmonic potential on all molecules, thus restricting the phase space accessible by the system. Further, the system phase space may have also been limited by neglect of thermal expansion. Finally, the use of a simulation cell (as shown in Figure 3-1) with edges and corners could lead to unrealistically high mobility in surface molecules.

3.2 Modeling Approach

The present modeling approach is based largely on the work of Yamamoto *et al.* [5], but invokes a different set of assumptions which are believed to represent the physics of the system more accurately. The approach is shown schematically in Figure 3-2, and the details of sampling schemes, criteria used to evaluate equilibration times, and computation of structural properties are discussed in this section.

3.2.1 Simulation Cell

As with the lattice dynamics study, simulation cells were developed to model thin crystalline slabs of extended-chain polyethylene molecules. As shown in Figure 3-3, the (100) Monte Carlo surface simulation cell differs from the corresponding lattice dynamics cell only in the cell dimension lateral to the surface. The broader Monte Carlo simulation cell was required to achieve uncorrelated motions in surface chains, as quantified in the results section. The current simulation cell construction does not suffer from edge- or corner-effects. In all cases, the input simulation cell for a given temperature was taken from the corresponding lattice dynamics results, thus explicitly accounting for thermal expansion. In the simulations, "interlayer spacings" (δx and δy in Figure 3-3) are computed as a measure of the expansion or contraction of the crystal lattice. The coordinates of a given layer were calculated by averaging

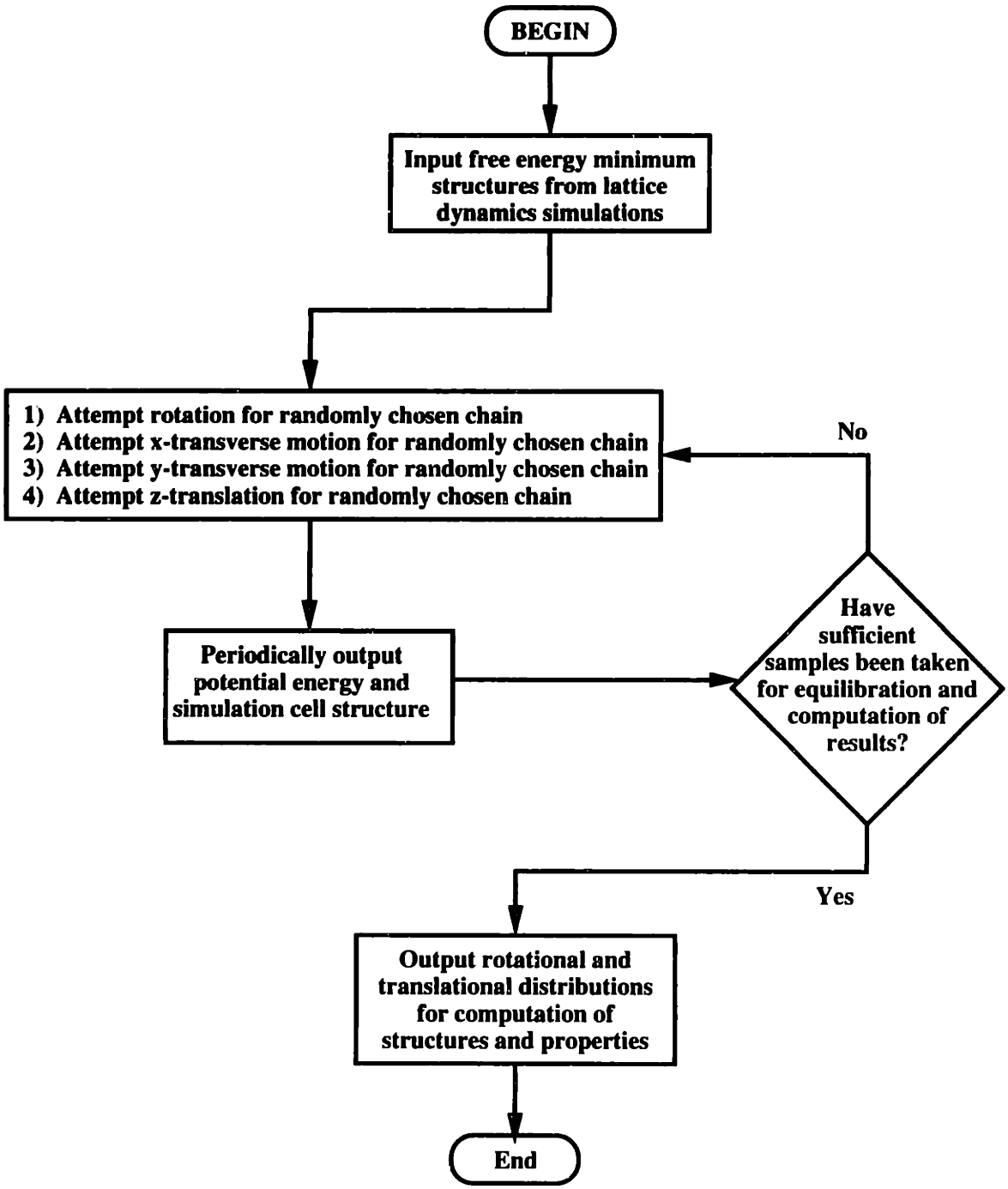

Figure 3-2: Flow chart outlining the Monte Carlo approach: details of the sampling scheme, the criteria used to determine acceptance of Monte Carlo moves, and the equilibration times and output distributions are given in the text.

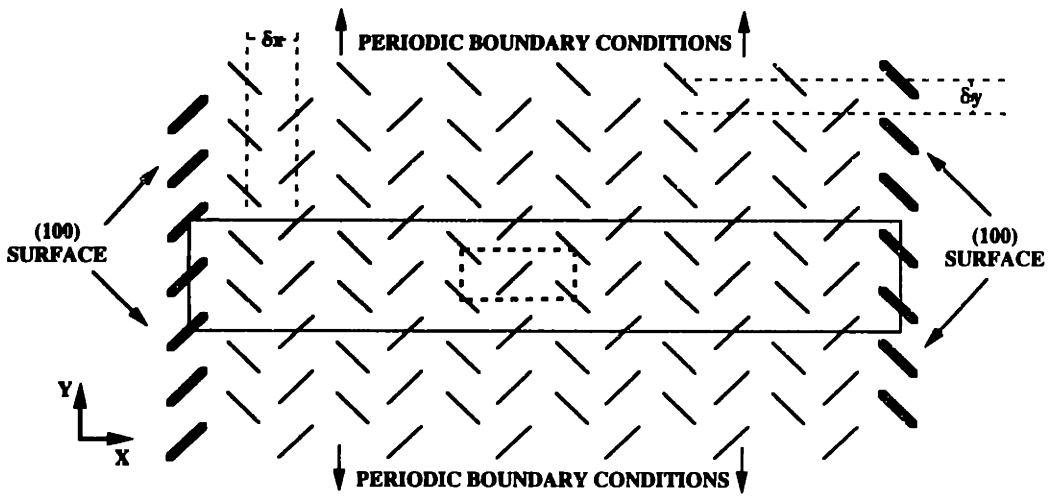

Figure 3-3: Monte Carlo simulation cell used to model the (100) surface. Diagonal lines are projections of the chain backbone as viewed down the chain axis; bold lines denote chains which lie on the (100) surface; the dotted rectangular line indicates the bulk crystal unit cell; the shaded region marks the boundary of the surface simulation cell; and periodic boundary conditions are considered in the direction shown (and in the direction of the chain axis). "Interlayer spacings", δx and δy, are calculated as the distance between neighboring (100) and (010) crystal planes, respectively.

the x- and y-coordinates of the center of masses of all chains in that layer. Eventually, analyses of larger simulation cells should be conducted to confirm that results are not dependent upon simulation cell size.

3.2.2 Sampling Scheme

Several different sampling schemes were considered in the development of the model. All schemes attempted chain rotations by perturbation of chain setting angles, and chain translations by perturbation of the three chain translational offset parameters. In general, sampling schemes considering small perturbations in chain rotation and translation generated high acceptance ratios, but also long simulation times due to inefficient sampling of phase space. However, consideration of significantly larger perturbations in chain rotation and translation required fewer Monte Carlo steps to adequately sample phase space, but low acceptance ratios led to prohibitively long simulations. The sampling scheme found to have most reasonable simulation times had intermediate acceptance ratios, roughly 50% for simulations at 300 K.

In a given Monte Carlo step, perturbations in the setting angle or translational offset parameter for a randomly selected chain were attempted according to:

$$\Theta_{i,new} = \Theta_{i,old} + \delta_{dof} \tag{3.1}$$

where $\Theta_{i,old}$ is the selected degree of freedom of chain i prior to the attempted move; $\Theta_{i,new}$ is the value after the attempted move; and δ_{dof} is the perturbation to the degree of freedom, a randomly chosen value from a uniform distribution bounded by $\pm\Delta$. The values of Δ for each degree of freedom are shown in Table 3.1. This sampling scheme does not artificially confine the motions of chains to be tethered at a lattice point, thus allowing for a more complete sampling of phase space.

The Monte Carlo simulations were conducted in the NPT ensemble, as the system volume fluctuates with translation of the surface chains. Attempted moves from state

Degree of Freedom	Δ
rotation	180°
x-translation	1.0 Å
y-translation	1.0 Å
z-translation	$c/2$

Table 3.1: Maximum perturbations considered in each attempted Monte Carlo step; c is the lattice spacing in the chain axis direction.

m to state n were accepted when the following inequality was satisfied [29]:

$$\exp\left(\frac{-\Delta H_{nm}}{kT}\right) > ran(0,1) \tag{3.2}$$

$$where: \Delta H_{nm} = \Delta E_{nm} + P\left(V_n - V_m\right) - kT \ln \frac{V_n}{V_m} \tag{3.3}$$

where ΔH_{nm} is the difference in a property similar to the enthalpy between states n and m; ΔE_{nm} is the change in potential energy in the step; P is an arbitrarily chosen system pressure; V_m and V_n are the simulation cell volumes before and after the attempted move; and $ran(0,1)$ is a randomly generated number between 0 and 1. The average positions of the center of mass of surface chains were used to compute the slab thickness, which in turn was used for calculating simulation cell volume. For the current sampling scheme, the magnitude of the third term in Equation 3.3 was several orders smaller than that of the other two terms.

Changes in intermolecular potential energy were evaluated using the KDG force field, and a 10 Å unit cell-based cutoff. Intramolecular potential energies were not computed, as the chain conformations remained rigid throughout the simulation. Longer cutoffs were necessary in lattice dynamics simulations as the intermolecular energy and its first and second derivatives were found to converge at much longer cutoffs than for ΔE_{nm}. Since the lateral dimension of the simulation cell is roughly equal to the potential energy cutoff distance, every Monte Carlo step actually considered multiple chain motions, thus modeling a system slightly different from that of isolated chain movements. To assess the difference between these two scenarios,

individual potential energy calculations were performed for a randomly selected set of Monte Carlo moves, and ΔE_{nm} was found to differ less than 0.1% for the two systems for all moves considered, thus indicating that the two different approaches sample virtually identical regions of phase space.

The system pressure strongly influenced the acceptance criteria of attempted moves, and ultimately the simulation results. At zero pressure, Equation 3.3 is determined solely by the potential energy effects, reducing Equation 3.2 to the same acceptance criteria used by Yamamoto *et al.* for NVT sampling. In this case, the crystalline slab configuration was found to be unstable, consistent with findings of Yamamoto *et al.* for simulations considering molecular motions of arbitrary magnitude and direction.[5] This behavior is attributed to the shallow potential energy barrier associated with removal of surface chains from the crystal, as displayed in Figure 3-4. However, at higher pressures, the crystalline slab remains stable over the entire sim-

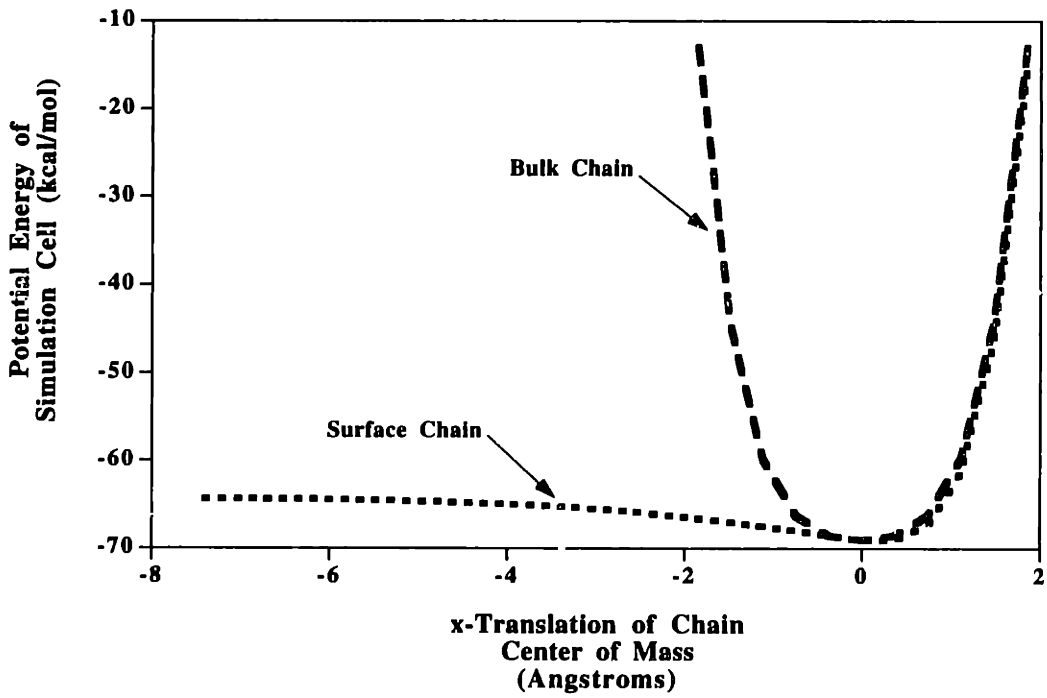

Figure 3-4: (100) Simulation cell energy as a function of the displacement of surface and bulk chains in the x-direction. The potential energy barrier for removing a surface chain from the crystal is less than 5 kcal/mol.

ulation, thus giving the simulation pressure physical significance: an external force required to overcome sublimation. At very high system pressures, the second term in Equation 3.3 favors the compression of simulation cells to unrealistically dense slabs. As will be discussed in the results section, a narrow range of pressure, roughly 5–10 atmoshperes, generates stable simulations.

3.2.3 Structure and Property Computations

Simulations were run for between 1.0×10^6 and 5.0×10^6 Monte Carlo steps, with samples taken every 500 steps. The equilibration period was determined by evaluating changes in the average of the potential energy, and by examining autocorrelation functions for slab thickness, interlayer spacings, and chain rotations and z-translations. Autocorrelation functions were calculated using the following equation [29]:

$$C_{\mathcal{A}\mathcal{A}}(\tau) = \langle \mathcal{A}(\tau)\,\mathcal{A}(0) \rangle = \frac{1}{\tau_{max}} \sum_{\tau_0=1}^{\tau_{max}} \mathcal{A}(\tau_0)\,\mathcal{A}(\tau_0 + \tau) \tag{3.4}$$

where $C_{\mathcal{A}\mathcal{A}}(\tau)$ is the autocorrlation function for property $\mathcal{A}$; $\mathcal{A}(\tau)$ is the property $\mathcal{A}$ evaluated after τ Monte Carlo steps; and τ_{max} is the total number of steps considered in the averaging period. The structural parameters substituted for $\mathcal{A}$ in Equation 3.4 are listed in Table 3.2. The system was considered equilibrated—all memory of the

Degree of Freedom	$\mathcal{A}$ (see Eqn. 3.4)
chain rotation	$\lvert\cos(\theta)\rvert$
z-translation	$\lvert\cos(Z\pi)\rvert$
interlayer spacing	$\delta x, \delta y$

Table 3.2: Structural properties used to evaluate autocorrelation functions; θ is the chain setting angle; Z is the z-translational offset parameter; and δx and δy are interlayer spacings between adjacent (100) and (010) molecular layers, respectively.

input configuration lost—when the autocorrelation functions reached their limiting values. Further discussion of equilibration is presented with the simulation results.

After the system had equilibrated, output distributions were compiled for the

following structural parameters: z-translational offset parameter and setting angle for each chain, slab thickness, and interlayer spacings. Ensemble averages and standard deviations in the structural parameters were determined. Correlation parameters were computed to determine whether simulation cell size may have introduced correlated motions, and were calculated as [29]:

$$C_{\mathcal{AB}} = \frac{\langle \delta\mathcal{A}\delta\mathcal{B} \rangle}{\sigma(\mathcal{A})\,\sigma(\mathcal{B})} \tag{3.5}$$

where $C_{\mathcal{AB}}$ is a measure of correlation between structural parameters $\mathcal{A}$ and $\mathcal{B}$, and the other terms in Equation 3.5 are given by [29]:

$$\delta\mathcal{A} = \mathcal{A} - \langle \mathcal{A} \rangle_{ens} \tag{3.6}$$

$$\sigma^2(\mathcal{A}) = \langle \mathcal{A}^2 \rangle_{ens} - \langle \mathcal{A} \rangle_{ens}^2 \tag{3.7}$$

The instantaneous fluctuation in property $\mathcal{A}$ is given by Equation 3.6, and the standard deviation of the fluctuations is given by Equation 3.7. Rotational correlation was assessed by replacing $\mathcal{A}$ with the cosine of the setting angle; z-translational correlation using the z-translational offset parameter; and transverse correlation by considering $\langle r^2 \rangle$. These equations were used to determine the correlation between various pairs of chains in the crystalline slab. In all cases, correlation parameters are bounded by 0 and 1, with values near 1 indicating significant correlation.[29]

3.3 Results

Investigative Monte Carlo simulations were completed for the (100) surface at temperatures of 100, 200, and 300 K, following the modeling approach presented above. The remainder of this section summarizes findings regarding the effect of pressure on the simulations, followed by the acceptance ratios, equilibration behavior, and structural properties computed for simulations of the (100) surface.

3.3.1 Effect of Pressure

As shown in Equations 3.2 and 3.3, the magnitude of the simulation pressure affects the acceptance criteria for a given Monte Carlo step, and thus determines the system phase space accessible in the simulation. The impact of the system pressure on the results for (100) simulations at 300 K are summarized in Figure 3-5. As shown, for pressures below 1.0 atmospheres (0.1 GPa), the crystalline slab configuration was

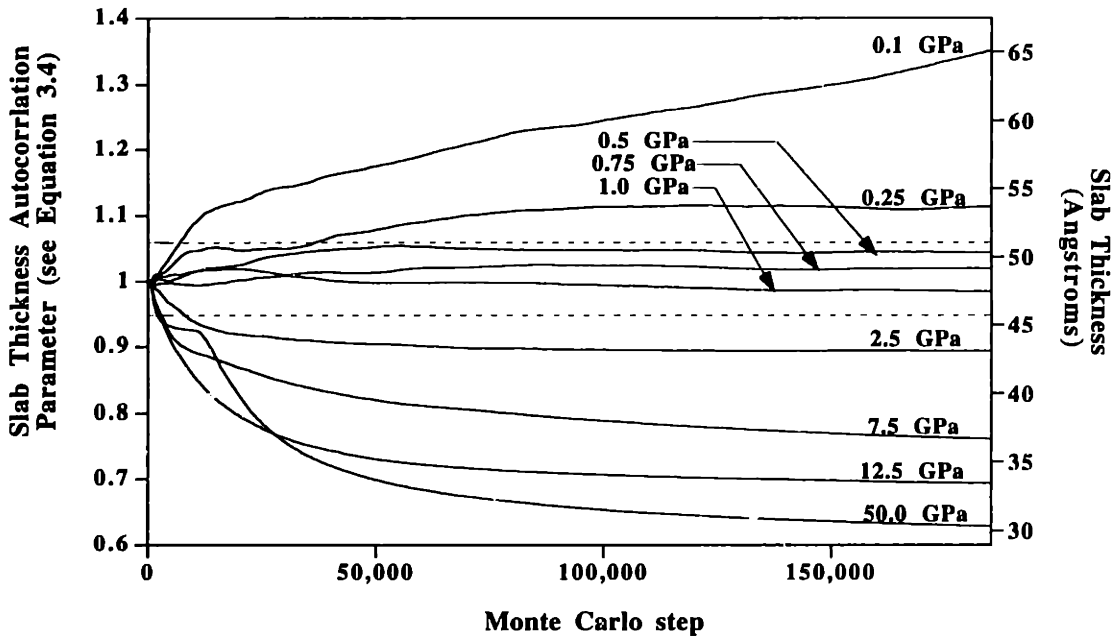

Figure 3-5: Equilibrated slab thickness and autocorrelation function for slab thickness (see Equation 3.4) for (100) surface simulations at 300 K as a function of pressure. Dashed lines mark the slab thicknesses ±5% those found from the lattice dynamics study. Simulations with slab thicknesses equilibrating between these bounds are considered to be the most realistic.

unstable, with surface chains moving away from the crystal without limit. Stable slabs were observed at pressures greater than 1.0 atmosphere, but the converged structures for higher pressures exhibited unrealistically high lattice compression.

To define bounds of simulation pressures which give realistic results, it was assumed that lattice expansion or contraction for the crystalline slabs would not exceed ±5% the vibrational free energy minimum structures determined in the lattice dynamics study. For simulations of the (100) surface at 300 K, pressures between 5–10

atmospheres (0.5–1.0 GPa) were found to fit this criteria, as shown in Figure 3-5. Unless otherwise noted, all results in the remainder of this paper are based on simulations conducted using a pressure of 5 atmospheres.

3.3.2 Acceptance Ratios

The sampling scheme was derived such that roughly 50% acceptance was observed for (100) surface simulations at 300 K. According to Equation 3.3, lower temperatures decrease acceptance rates by virtue of both the decreased Boltzmann factor (kT) and the increased values of potential energy changes (ΔE_{nm}) resulting from the more compressed lattice. A summary of the acceptance ratios, broken down by bulk and surface chains, degree of freedom, and temperature, is shown in Table 3.3. As expected, acceptance ratios were highest for the 300 K simulations and were also

Degree of Freedom	Chains	100 K	200 K	300 K
Rotation	Surface	13%	27%	40%
	Bulk	6%	14%	27%
	Overall	7%	16%	29%
x-translation	Surface	42%	55%	65%
	Bulk	34%	48%	58%
	Overall	35%	49%	59%
y-translation	Surface	51%	64%	75%
	Bulk	37%	53%	65%
	Overall	39%	55%	66%
z-translation	Surface	52%	69%	80%
	Bulk	34%	59%	71%
	Overall	37%	61%	73%
All combined	Surface	40%	54%	64%
	Bulk	27%	43%	55%
	Overall	29%	45%	57%

Table 3.3: Acceptance ratios observed in simulation of the (100) surface at 5.0 atmospheres pressure broken down by degree of freedom and temperature. Surface chains are those in the outermost crystalline layer, all other chains are considered "bulk".

significantly higher for perturbations in surface chains. As a result of the sampling scheme employed, acceptance was also highest for z-translation of chains, and lowest

for chain rotations. However, this last trend is an outcome of the sampling scheme used and does not necessarily reflect the physics of the system.

3.3.3 Equilibration

The equilibration period was determined by monitoring the simulation cell potential energy and autocorrelation functions for several structural parameters. As shown in Figure 3-6 for the 300 K analysis of the (100) surface, the instantaneous potential

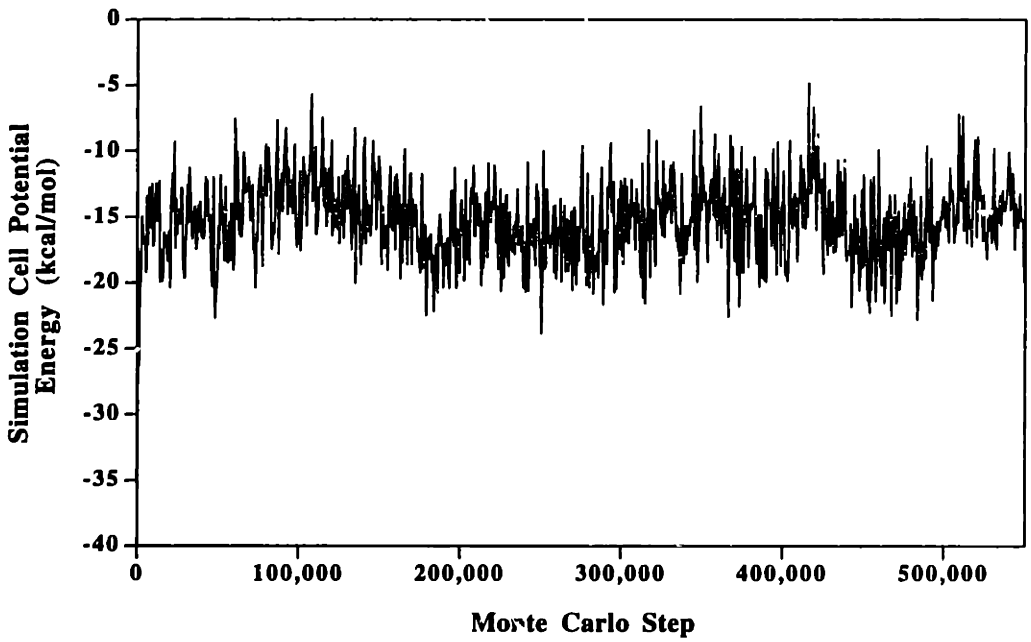

Figure 3-6: Simulation cell potential energy for the (100) surface analysis at 300 K as a function of Monte Carlo step.

energy of the simulation cell begins to oscillate about a steady equilibrium value within the first 200,000 Monte Carlo steps. Similar energy equilibration durations were observed for the 100 K and 200 K simulations.

The autocorrelation functions of the structural parameters listed in Table 3.2 reached limiting values well within 200,000 Monte Carlo steps as well. As shown in Figure 3-5, the crystal slab thickness reached stable values within the first 100,000 Monte Carlo steps for simulations at 5 atmospheres pressure, and the interlayer spac-

ing was found to have similar convergence behavior. Autocorrelation functions for the z-translation and rotation of chains are shown in Figure 3-7 and 3-8, respectively, for 100 K simulations at 5 atmospheres pressure. As shown, the z-translation of chains

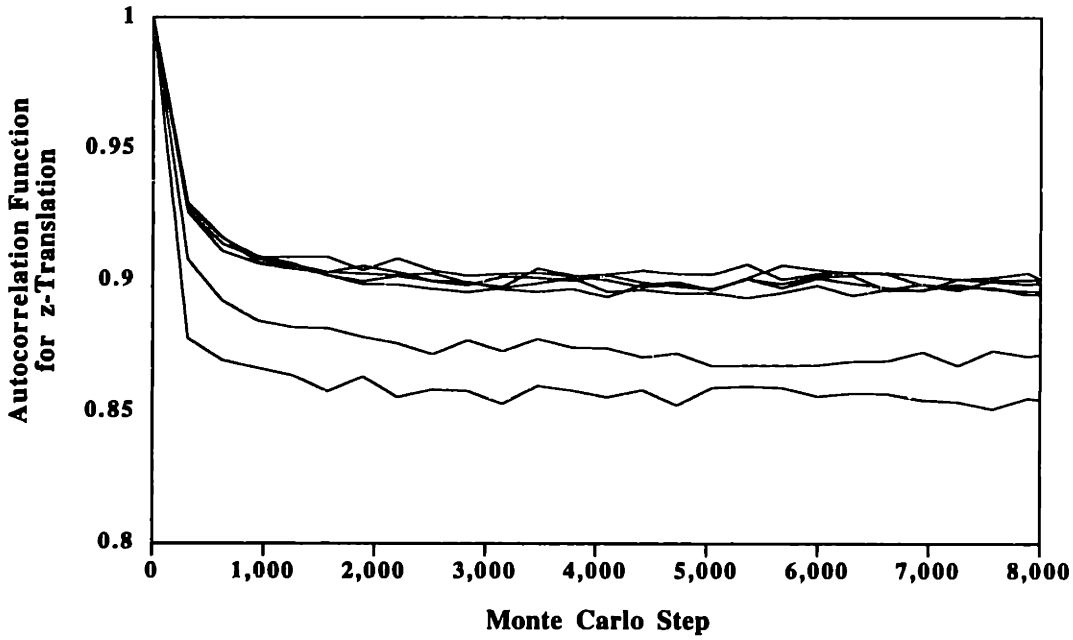

Figure 3-7: Autocorrelation functions for z-translation of chains from (100) surface simulations at 100 K and 5 atmospheres pressure. Plots are shown for seven chains located at different distances from the surface.

equilibrated well within the first 10,000 Monte Carlo steps, and chain rotations within roughly the first 60,000 Monte Carlo steps. Equilibration durations for the 200 K and 300 K are expected to be shorter by virtue of the higher acceptance ratios. Based on these findings, a conservative estimate of a 300,000 Monte Carlo step equilibration duration was assumed for all simulations.

3.3.4 Distributions of Structural Properties

Following system equilibration, samples from the simulation were taken every 500 Monte Carlo steps to compile output distributions of structural parameters. The distributions for the z-translation of chains as a function of temperature and depth into crystal are shown in Figure 3-9, with the standard deviations of the distributions given

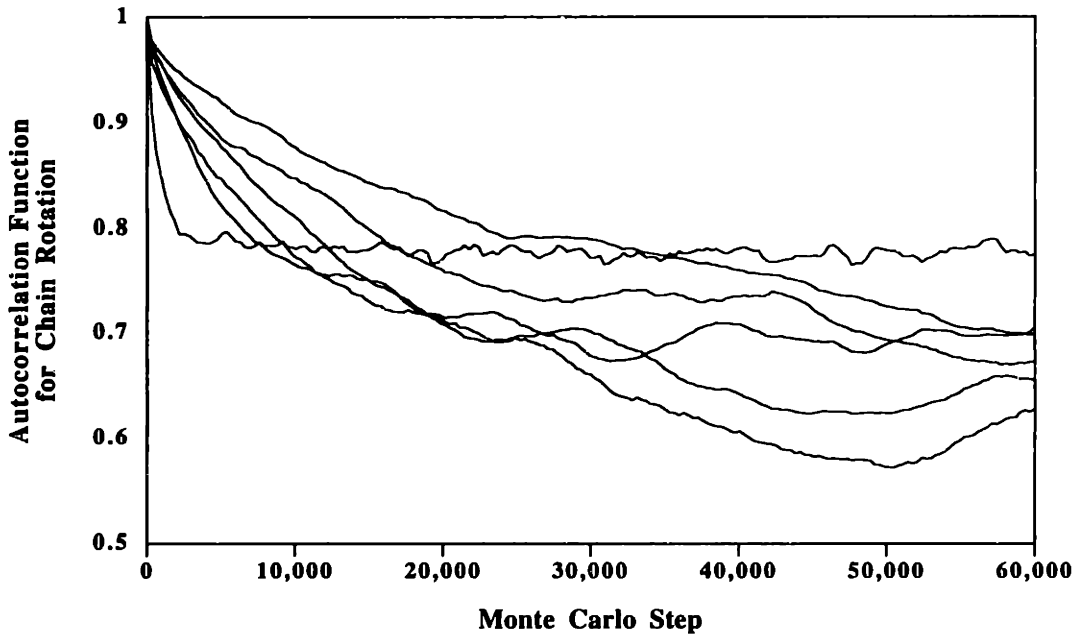

Figure 3-8: Autocorrelation functions for chain rotations from (100) surface simulations at 100 K and 5 atmospheres pressure. Plots are shown for seven chains located at different distances from the surface.

in Table 3.4. Significant z-translational disorder exists for all chains in the crystal, even at temperatures of 100 K. At 300 K, the chains have little barrier to motions in the c-axis direction, and the distribution of z-translational offset parameters is nearly uniform throughout the crystal. The magnitude of disorder is partly the result of the simulation cell dimension in the direction of the chain axis, and simulation cells with more than two repeat units per chain are expected to predict more ordered systems for z-translation. It should be noted that surface chains exhibit marginally larger disorder than corresponding chains in the bulk, consistent with interpretations which can be made from the [0 0 1] phonon dispersion curves (see Figure 2-5, plots (a) and (b)) from the lattice dynamics study. The small perturbations in the [0 0 1] branch of the phonon dispersion curve by the presence of the surface suggests that the z-translation of surface chains is not significantly different than that observed in the bulk crystal.

The distribution of chain setting angles observed for the 100 K, 200 K, and 300 K, simulations at 5 atmospheres pressure are shown in Figures 3-10, 3-11, and 3-

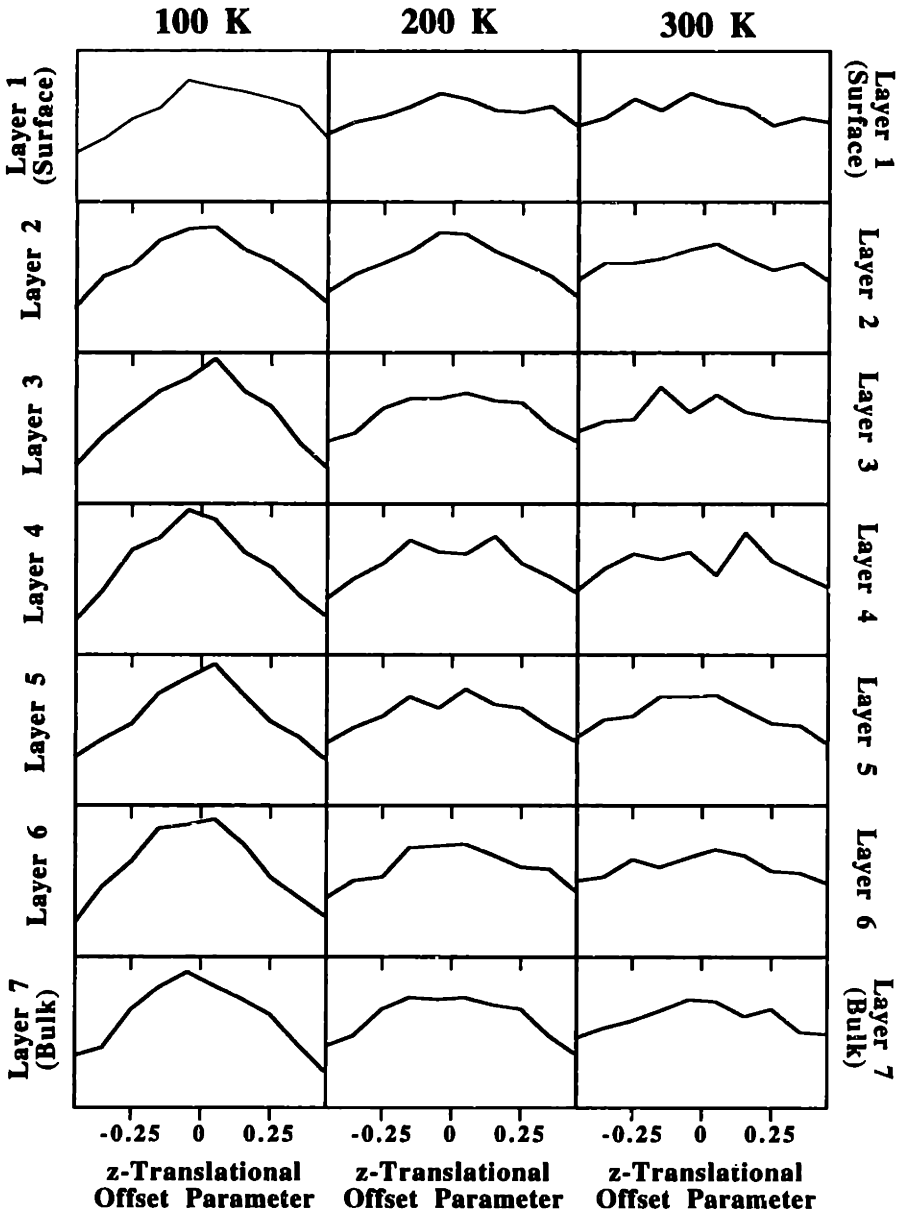

Figure 3-9: Normalized distributions of the z-translational offset parameter as a function of temperature and distance from the (100) surface; the vertical axes on all of the plots have the same bounds.

Molecular Layer	100 K	200 K	300 K
1 (Surface)	0.358	0.385	0.394
2	0.346	0.365	0.383
3	0.327	0.365	0.387
4	0.324	0.364	0.377
5	0.324	0.370	0.374
6	0.325	0.370	0.376
7 (Bulk)	0.324	0.365	0.379

Table 3.4: Standard deviations of the distributions of z-translational offset parameters, as a function of temperature and distance from the (100) surface.

12, respectively. The results at 100 K and 200 K both indicate a crystal with a four-site distribution of chain setting angles, while at 300 K rotational disorder exists throughout the crystalline slab. At 100 K and 200 K, the distributions of bulk chain setting angles centered at 45° and 135° are quite broad, and surface chains readily sample from all setting angles. Significant discrepancies are observed between the results of the present study, and those of the study by Yamamoto *et al.*[5] In the previous study, virtually no rotational disorder was observed throughout the crystal at 100 K, and bulk setting angle distributions were extremely narrow, even at 200 K.[5] The enhanced rotational freedom found in the present work is believed to result from chain rotations being strongly coupled to the translational motions of neighboring chains. As the previous study imposed unrealistic constraints on chain translation, the chain rotations observed were also artificially restricted. Thus, limiting translational motion by constraining chains to lattice points restricts the rotational phase space that can be sampled in a simulation, a conclusion expected to apply to most simulations of condensed phases of rod-like molecules.

Ryckaert and Klein have conducted several molecular dynamics studies of the high temperature behavior of n-alkane crystals, and have found four-site distributions of chain setting angles for systems at temperatures greater than 325 K, with two-site distributions at lower temperatures.[30-32] The four-site distributions predicted for 100 K and 200 K crystals in the present work are not necessarily inconsistent with the results of Ryckaert and Klein, as efficient Monte Carlo simulations can sample regions

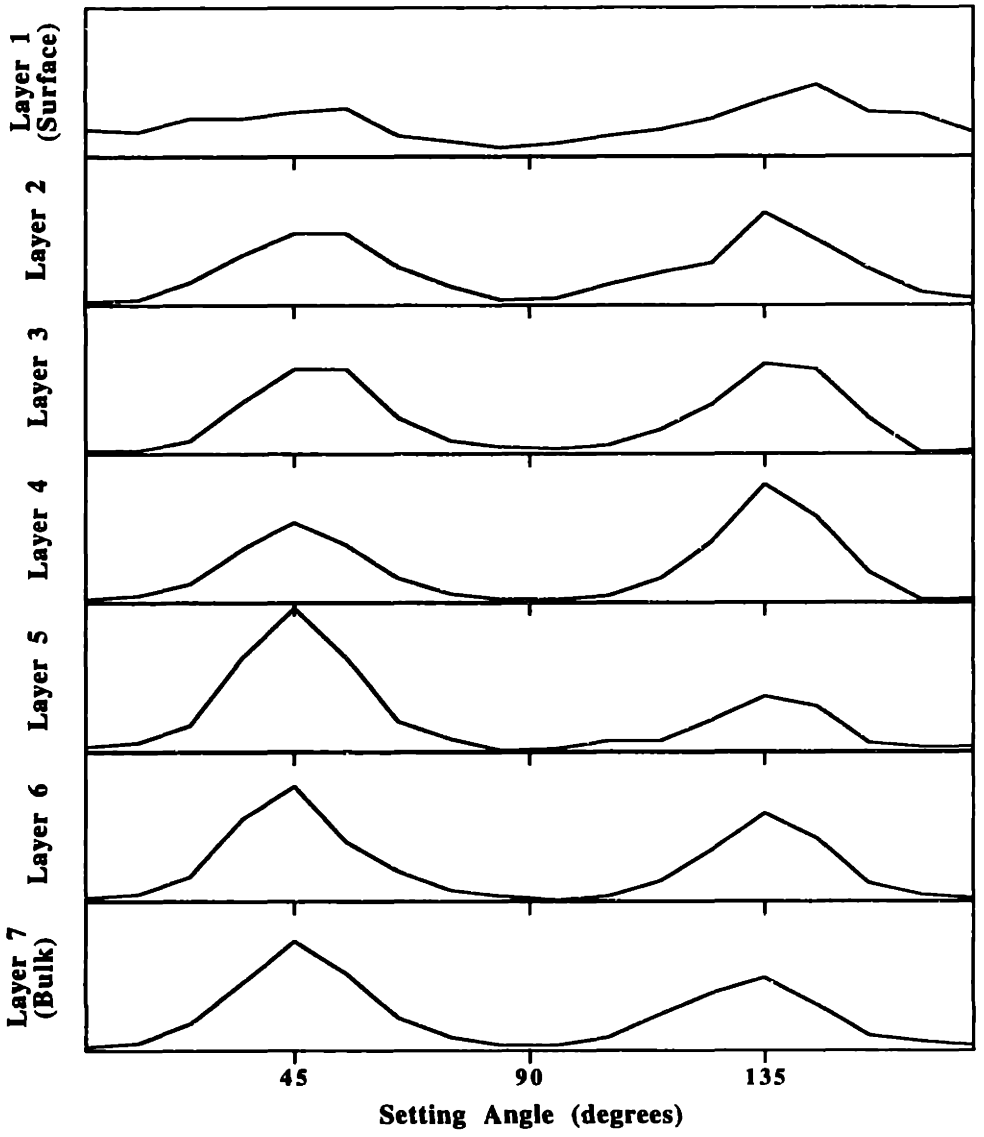

Figure 3-10: Distributions of chain setting angles observed in 100 K simulation at 5 atmospheres pressure, as a function of depth into crystal.

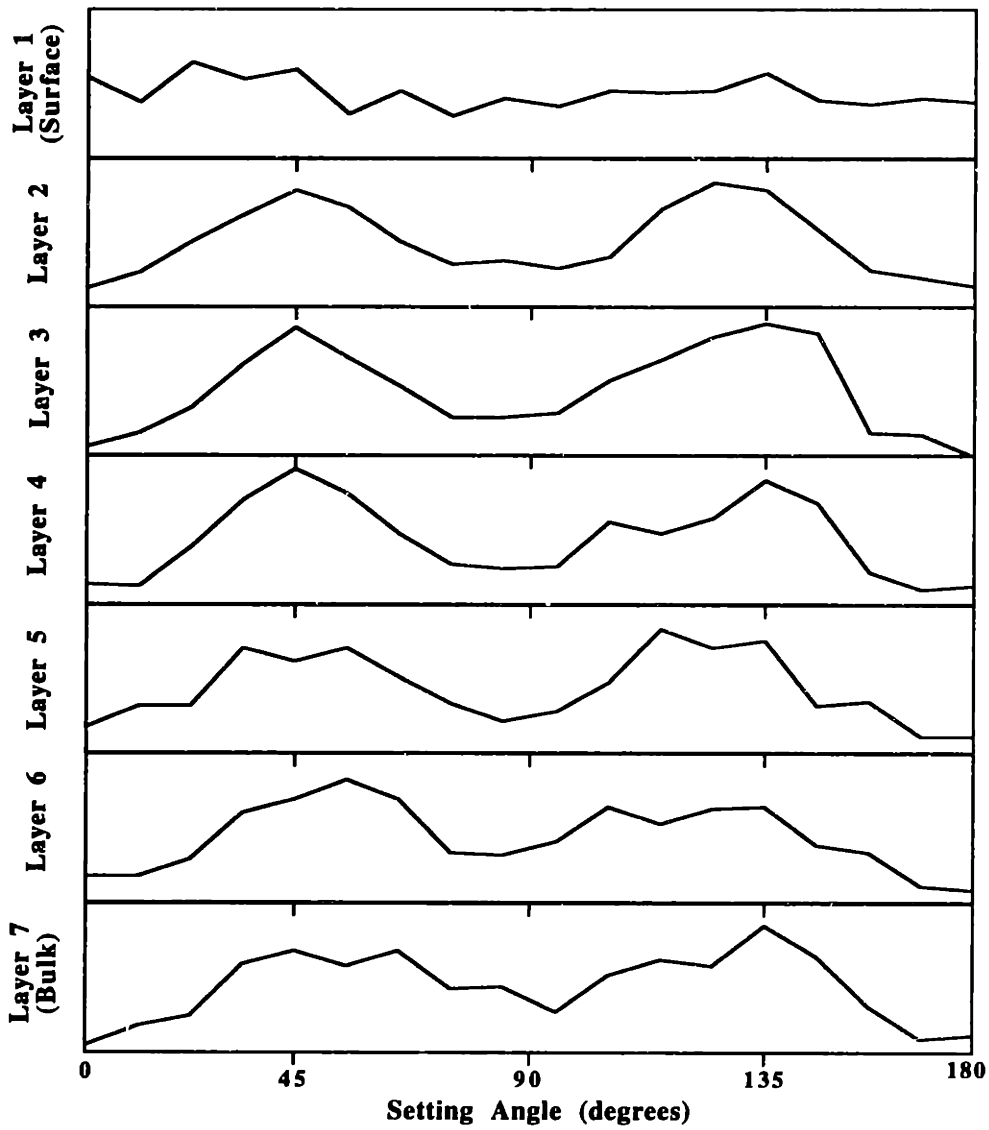

Figure 3-11: Distributions of chain setting angles observed in 200 K simulation at 5 atmoshperes pressure, as a function of depth into crystal.

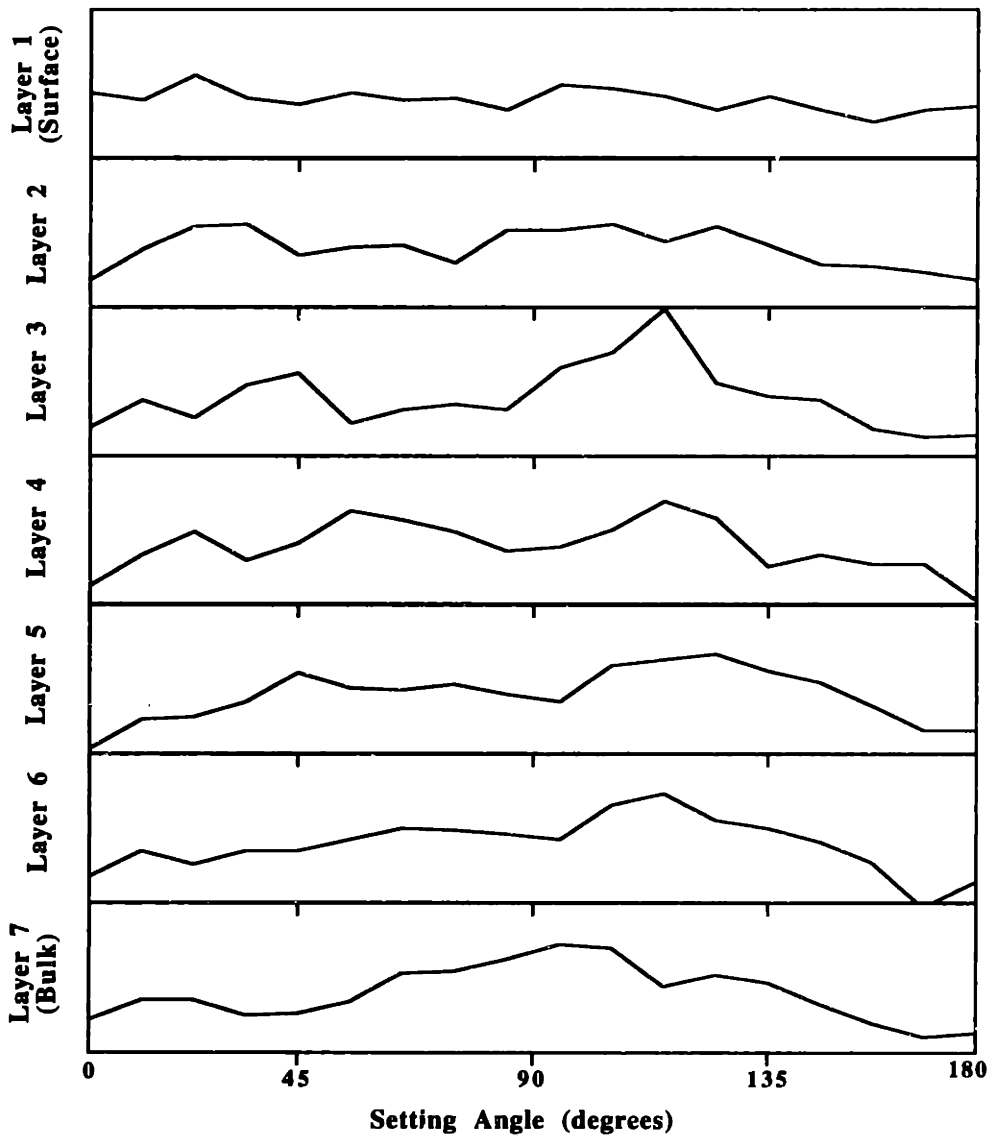

Figure 3-12: Distributions of chain setting angles observed in 300 K simulation at 5 atmospheres pressure, as a function of depth into crystal.

of phase space that may be separated by high energy barriers, whereas the phase space sampled in molecular dynamics is restricted by short simulation times and potential energy barriers.[29] However, the featureless chain setting angle distribution predicted in the 300 K simulations at 5 atmospheres pressure (see Figure 3-12) is inconsistent with the findings of Ryckaert and Klein [30], and the discrepancy cannot be explained by the different simulation techniques, but is resolved in the next paragraph upon consideration of interlayer spacings.

The distribution of interlayer spacings was monitored as a measure of the translational motion of the crystalline chains, and is summarized in Table 3.5. In all

Layers	100 K	200 K	300 K
1–2	3.74 (0.174)	3.90 (0.270)	4.03 (0.355)
2–3	3.67 (0.157)	3.81 (0.250)	3.93 (0.335)
3–4	3.66 (0.149)	3.81 (0.243)	3.93 (0.305)
4–5	3.67 (0.156)	3.81 (0.243)	3.93 (0.327)
5–6	3.66 (0.159)	3.83 (0.251)	3.95 (0.290)
6–7	3.68 (0.159)	3.83 (0.243)	3.95 (0.335)

Table 3.5: Equilibrium average interlayer spacings normal to the (100) surface, in Å, and standard deviations (in parentheses) by crystal layer and temperature. Layer 1 is a surface layer, and layer 7 is embedded in the bulk crystal.

cases, lattice expansion of between 2–3% was observed in the outermost crystalline layer. The enhanced rotations of surface chains discussed earlier is expected to be coupled to surface expansion effects. It should be noted that the magnitude of the surface expansion predicted in this model is likely determined by the simulation pressure. Lattice dynamics simulations of the bulk polyethylene crystal have found lattice spacings of 3.68 Å, 3.73 Å, and 3.78 Å, for the bulk crystal at 100 K, 200 K, and 300 K, respectively. Thus, a simulation pressure of 5 atmospheres reproduces bulk crystal lattice spacings at 100 K, but leads to an overall lattice expansion of nearly 5% for the 300 K simulations. To attain better consistency with bulk lattice spacings, 300 K simulations were repeated using various simulation pressures, and average equilibrium interlayer spacings in the interior of the crystal of 3.78 Å were observed

for simulation pressures of 7.5 atmospheres. The chain setting angle distribution for these simulations is shown in Figure 3-13. In contrast to the results depicted in

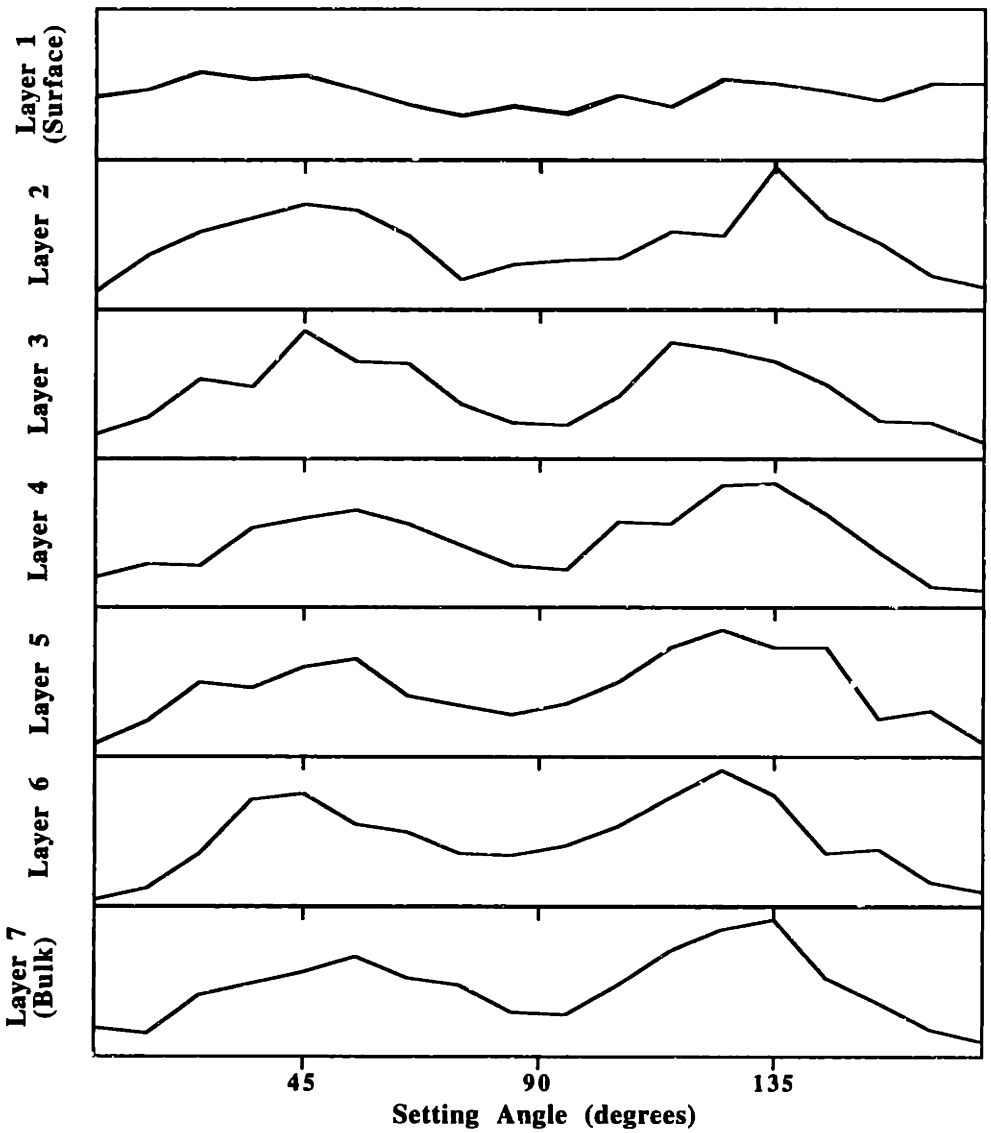

Figure 3-13: Distributions of chain setting angles observed in 300 K simulation at 7.5 atmospheres pressure, as a function of depth into crystal.

Figure 3-12, a four-site chain setting angle distribution was observed for the 300 K simulations when simulation pressures were chosen such that bulk lattice spacings achieved those predicted by the lattice dynamics results. These simulated results are consistent with those of Ryckaert and Klein [30], and further prove that the choice of simulation parameters and sampling schemes is critical in the prediction of realistic

results.

3.3.5 Correlation Parameters

Correlation parameters were calculated to assess the degree of correlated rotations, transverse motions, and z-translational motions among different pairs of chains in the simulations using Equation 3.5. Selected results for the analysis of the z-translation of chains are shown in Table 3.6. The tabulated correlation parameters suggest that

Temperature	Surface Chains	Bulk Chains
100 K	0.0029	0.022
200 K	0.0084	0.0087
300 K	0.0074	0.011

Table 3.6: z-Translation correlation parameters, C_{AB}, calculated for two neighboring chains in the center of the crystalline slab, and for two adjacent chains on the (100) crystal surface; thus, A and B refer to the z-translational offset parameters for the two chains of interest.

z-translational motions in chains are virtually uncorrelated from the motion in a neighboring chains. Similar results are observed in the correlation parameters of the other degrees of freedom.

Chapter 4

Discussion

Surfaces of the extended-chain crystalline slabs considered in the present study are ideal representations of actual lateral surfaces observed in polymer crystals, as most crystals of flexible chain polymers grown from dilute solution form lamellar structures (an ideal schematic is shown in Figure 1-1). It is important to consider how structures and properties predicted for the extended-chain crystals might apply to such chain-folded systems.

With regards to the structure of chains at the lateral surface, the presence of chain folds is expected to perturb the free energy minimum structures over a short "interfacial thickness", δ. Results from the present work and from simulations of the amorphous polymer-vacuum interface [23] indicate that interfacial thicknesses between condensed polymer phases and vacuum are on the order of 10 Å. Extending this finding to the crystal fold surface, isolated polymer crystals in vacuum may be represented schematically as shown in Figure 4-1. In this diagram, chain segments embedded in the bulk crystal (Region 3) are expeceted to assume the bulk structures as calculated by previous work and confirmed by experiment [13, 24], and structures in the interfacial region of the lateral surface (Region 2) should exhibit the structures of surface chains predicted in this study. Only lateral surface chains in the interfacial region near the chain fold surface (the shaded region on the diagram) are expected to have structures different from those predicted in the present work. Since polyethylene crystals grown under atmospheric pressure exhibit lamellar thicknesses on the order

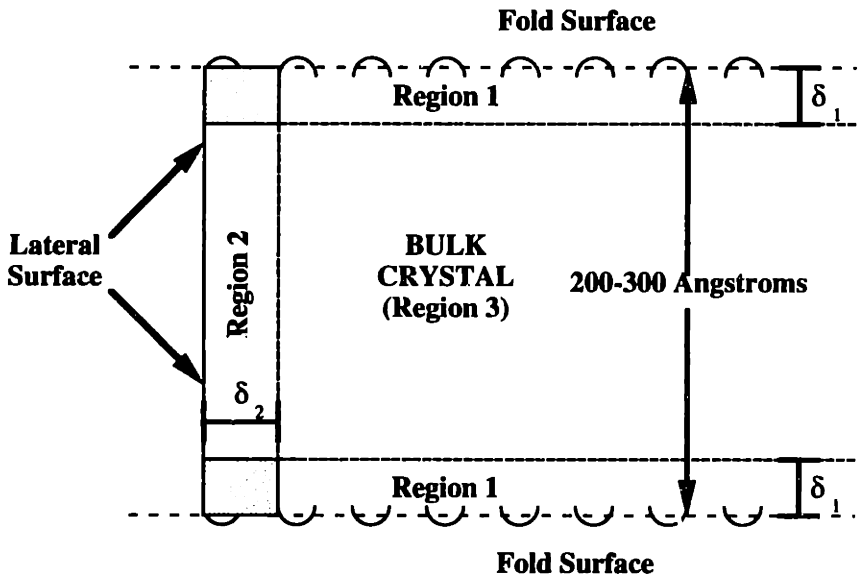

Figure 4-1: Schematic of an isolated lamellar crystal, with only tight adjacent folds shown. The structure and properties of crystalline segments in Region 1 and 2 are perturbed from bulk values by the presence of the fold surface and the lateral surface, respectively; chain segments in Region 3 assume bulk crystal values; and the structure of chain segments in the shaded regions are expected to be perturbed by both the lateral and fold surfaces. Interfacial thickness, δ_1 and δ_2 (both not to scale with the sketched lamellar thickness, are shown.

of 200–300 Å [33], and interfacial thicknesses of 10 Å are assumed, the structure of at least 90% of the exposed lateral surface chains in a lamellar crystal are expected to be nearly equal those computed for the extended-chain crystal in the present work.

With regards to surface properties, the impact of the fold surface on lateral surface properties can be assessed by considering the effects chain folds may have on the normal mode vibrational frequencies, particularly for lattice modes. Such analyses have been done previously by comparing the experimental vibrational frequency spectra of lamellar polyethylene crystals to extended-chain n-alkane crystals, which are known to exhibit great structural similarity to polyethylene crystals, except without chain folding.[34] The study showed a deviation in as much as 10% in the transverse acoustic vibrational mode frequencies between the two different crystals, with the other lattice modes and the intramolecular modes exhibiting significantly smaller deviations.[34] These results are expected to be applicable to both Regions 2 and 3, but vibrational modes in Region 1 likely show significant departures from those calculated for the bulk crystal. Such studies suggest that the impact of chain folds on bulk vibrational frequencies, and therefore properties, may indeed be marginal, and that the properties of the lateral surface calculated in the present study should serve as a good estimate for the properties observed in lamellar crystals.

Chapter 5

Conclusion

5.1 Summary of Findings

The structure and properties of the (100), (010), and (110) lateral crystal surfaces of extended-chain polyethylene crystals were determined from first principles at temperatures of 0–300 K using both consistent quasi-harmonic lattice dynamics and Monte Carlo simulation methods.

The main assumptions in the lattice dynamics study were the use of an empirically derived force field to quantify the interactions of the atoms in surface simulations and the modeling of the thermal motions of the system as quasi-harmonic. These approximations are expected to be less accurate above about 200 K. Nevertheless, the results suggest a very consistent picture for the structure and relative stability of the low index faces of the lateral crystallographic surfaces over the entire temperature range considered. In particular, only modest rotations of chains are found near the surface, which is confined to the 2–3 outermost layers. There is no indication of lattice expansion in the vicinity of the surface. The (110) surface is found to be at least 15% more stable than either the (100) or (010) surfaces, primarily due to lower vibrational energy and vibrational entropy, both associated with the denser packing of chains at the surface. The temperature dependence of the surface properties results primarily from low-frequency, large-amplitude lattice mode motions.

Preliminary results from Monte Carlo simulations complement the findings of the

lattice dynamics study. Simulations of the (100) surface at 5 atmospheres pressure show significant rotational disorder of surface chains at 100 K and 200 K, with the magnitude of disorder rapidly decreasing with depth into the crystal. Complete rotational disorder is observed throughout the crystal at 300 K and 5 atmospheres pressure, but unrealistically high lattice spacings were also observed in the center of the slab. Four-centered chain rotational distributions were observed at 300 K for simulations at 7.5 atmospheres pressure, along with lattice spacings more representative of the bulk crystal. At 5 atmospheres pressure, bulk lattice spacings for the 100 K simulation were found to be nearly identical to those determined using lattice dynamics, with the exception of 2–3% expansion observed in the interlayer spacing at the surface. Comparison of the results to previous studies has shown that the rotational and translational motions of chains are intimately coupled, and that sampling schemes which restrict either degree of freedom may severely limit the phase space sampled in the system.

5.2 Recommendations for Future Work

Continued studies of the polymer crystal-vacuum interface can provide valuable information on the structure and properties of the lateral crystal surface. The current lattice dynamics results can be validated by investigative Monte Carlo or molecular dynamics studies, used to gauge the validity of the harmonic approximaion at surfaces of polymer crystals. For example, trajectories of atomic motions, and distributions of atomic motions, can be readily calculated in lattice dynamics simulations, and these can be compared to corresponding distributions compiled from a Monte Carlo study. In any case, a more comprehensive Monte Carlo study may also be helpful in comparing the surface disorder between the different surface habits.

Further, in both the lattice dynamics and Monte Carlo simulations, intramolecular degrees of freedom of the surface chains were not considered. Relaxing this assumption allows for the investigation of surface chain conformations other than those of the minimized bulk crystal, and may lead to interesting conclusions regarding sur-

face conformational disorder. Extending this approach, one may eventually conduct "crystallization studies", similar to those of Patel and Farmer [3], by examining the potential and free energy barriers associated with attaching a distant chain to the lateral crystal surface, and moving adsorbed chains into crystalline registry.

With some modifications to the current approach, the effects of solvent on the lateral crystal surface structure and properties could be evaluated, and such information would prove valuable for more direct applications to polymer crystallization theory. This can be best achieved by incoporating Monte Carlo or molecular dynamics simulation techniques to consider crystal-solvent interfaces. Previous studies have employed a mean field to characterize solvent effects on crystal surface properties [35]; but other work has suggested that crystal surface structure is largely determined by local molecular interactions [36], thus implying that mean field techniques may fail to consider important local structure effects. As such, a fully atomistic model of the crystal-solvent interface is recommended to best capture the surface structure and properties. Such a model would be computationally intensive, but could yield lateral surface properties computed from first principles for any polymer crystal-solvent pair, provided accurate force fields exist to quantify the intermolecular interactions.

Credibility in the present study can also be established through experimental validation of the simulated structures and properties. It is recommended that surface properties be measured directly, as opposed to using crystallization theories or empirical relations in conjunction with experimental data. Surface structure may be experimentally observed using atomic force microscopy, and surface free energies may be derived using contact angle experiments. In either case, samples must be prepared such that the lateral crystal surface is significantly isolated from amorphous regions, which may be accomplished by using epitaxially grown crystals, or crystal grown under high pressure.

With thorough data available characterizing the lateral crystal surface, and eventually the folded crystal surface, much of the uncertainty surrounding the current polymer crystallization theories may be resolved, and it is in this area where the present research holds great promise. For many years, predictions based on the cur-

rently accepted polymer crystallization theories are often predicated on the lack of data quantifying key parameters, such as lateral and fold surface free energies, and equilibrium melting temperatures. With thorough data becoming available on these parameters from studies such as this, it is hoped that more accurate predictions within the framework of current polymer crystallization theories can be made, or that more accurate theories may eventually be derived to better accommodate the data becoming available.

Bibliography

[1] J. Hoffman and J. Laurtizen. *J. Research NBS*, 64A:73, 1960.

[2] J.D. Hoffman, G.T. Davis, and J.I. Lauritzen. *Treatise on Solid State Chemistry*, volume 3, pages 497–614. Plenum, New York, 1976.

[3] A.K. Patel and B.L. Farmer. *Polymer*, 21:153, 1980.

[4] I.C. Sanchez and E.A. DiMarzio. *Macromolecules*, 4:677, 1971.

[5] T. Yamamoto, M. Hikosaka, and N. Takahashi. *Macromolecules*, 27:1466, 1994.

[6] G.L. Liang, D.W. Boid, B.G. Sumpter, and B. Wunderlich. *Makromol. Chem., Theory Simul.*, 2:245, 1993.

[7] N. Karasawa, S. Dasgupta, and W.A. Goddard. *J. Phys. Chem.*, 95:2260, 1991.

[8] F.J. Medellin-Rodriguez, P.J. Phillips, and J.S. Lin. *Macromolecules*, 28:7744, 1995.

[9] C.F. Fan and T. Cagin. *J. Chem. Phys.*, 103:9053, 1995.

[10] D.G. Thomas and L.A.K. Staveley. *J. Chem. Soc.*, page 4569, 1952.

[11] D.K. Owens and R.C. Wendt. *J. App. Polymer Sci.*, 13:1741, 1969.

[12] R.H. Dettre and R.E. Johnson. *J. Colloid Interface Sci.*, 21:367, 1966.

[13] D.J. Lacks and G.C. Rutledge. *J. Phys. Chem.*, 98:1222, 1994.

[14] N. Karasawa and W.A. Goddard. *J. Phys. Chem.*, 93:7320, 1989.

[15] J.E. Black. *Structure and Dynamics of Surfaces I*, pages 153–198. Springer-Verlag, Berlin, 1986.

[16] G. Venkataraman, L.A. Feldkamp, and V.C. Sahni. *Dynamics of Perfect Crystals*, pages 1–165. MIT Press, Cambridge, 1975.

[17] R.F. Wallis. *Dynamical Properties of Solids*, pages 451–507. North-Holland Publishing Company, Amsterdam, 1975.

[18] D.J. Lacks and G.C. Rutledge. *J. Chem. Phys.*, 101:9961, 1994.

[19] J.F. Lutsko, D. Wolf, and S. Yip. *J. Chem. Phys.*, 88:6525, 1988.

[20] F.W. de Wette. *Interatomic Potentials and Simulation of Lattice Defects*, pages 653–671. Plenum, New York, 1972.

[21] D.A. McQuarrie. *Statistical Thermodynamics.* Harper & Row, New York, 1973.

[22] W.H. Press, B.P. Flannery, S.A. Teukolsky, and W.T. Vetterling. *Numerical Recipes: The Art of Scientific Computing*, pages 274–334. Cambridge University Press, Cambridge, 1986.

[23] K.F. Mansfield and D.T. Thedorou. *Macromolecules*, 23:4430, 1990.

[24] R.E. Allen, G.P. Alldredge, and F.W. deWette. *Phys. Rev. B*, 4:1648, 1971.

[25] R.E. Allen, G.P. Alldredge, and F.W. deWette. *Phys. Rev. B*, 4:1661, 1971.

[26] W.L. Peticolas, G.W. Hibler, J.L. Lippert, A. Peterlin, and H. Olf. *App. Phys. Let.*, 18:87, 1971.

[27] E. Passaglia and F. Khoury. *Polymer*, 25:631, 1983.

[28] N. Metropolis, A.W. Rosenbluth, M.N. Rosenbluth, A.H. Teller, and E. Teller. *J. Chem. Phys.*, 21:1087, 1953.

[29] M.P. Allen and D.J. Tildesley. *Computer Simulation of Liquids*, pages 1–239. Oxford University Press, New York, 1987.

[30] J.P. Ryckaert and M.L. Klein. *J. Chem. Phys.*, 85:1613, 1986.

[31] J.P. Ryckaert and M.L. Klein. *Phys. Rev. Lett.*, 58:698, 1987.

[32] J.P. Ryckaert and M.L. Klein. *Molecular Physics*, 67:957, 1988.

[33] W.O.Statton and P.H. Geil. *J. Appl. Polymer Sci.*, 3:357, 1960.

[34] C. Wu and M. Nicol. *J. Chem. Phys.*, 58:5150, 1973.

[35] X. Liu. *J. Chem. Phys.*, 102:1373, 1995.

[36] J.Q. Broughton and G.H. Gilmer. *J. Chem. Phys.*, 79:5095, 1983.